Fluorescence Characteristics of 5-Carboxytetramethylrhodamine Linked Covalently to the 5′ End of Oligonucleotides: Multiple Conformers of Single-Stranded and Double-Stranded Dye-DNA Complexes

György Vámosi,*§ Christoph Gohlke,*# and Robert M. Clegg*
*Max Planck Institute for Biophysical Chemistry, Department of Molecular Biology, D-37077 Göttingen, Germany; #Department of Molecular Biology, Institute for Molecular Biotechnology e.V., D-07745 Jena, Germany; and §Department of Biophysics, Medical University of Debrecen, H-4012 Debrecen, Hungary

ABSTRACT Fluorescence steady-state and lifetime experiments have been carried out on duplex and single-stranded DNA molecules labeled at the 5′ ends with 5-carboxytetramethylrhodamine (TMRh). The temperature and ionic strength of the solutions were varied over large ranges. The results reveal at least three well-defined states of the TMRh-DNA molecules for the single-stranded as well as for the double-stranded DNA molecules. Two states are fluorescent, with lifetimes in the range of 0.5–1 ns and 2.5–3 ns. A third state of TMRh-DNA does not fluoresce (a dark species of TMRh-DNA). The distribution of the TMRh-DNA molecules among these three states is strongly temperature and ionic strength dependent. Estimates are made of some reaction parameters of the multistate model. The results are discussed in terms of the photophysics of TMRh, and consequences of the multiple conformers of TMRh-DNA for studies involving fluorescence studies with TMRh-labeled DNA are considered.

INTRODUCTION

Well-defined sequences of DNA/RNA oligomers are now synthesized routinely, and fluorescence labels can be conjugated at specific positions of DNA oligomers. The increasing number of publications employing fluorophores that are covalently conjugated to distinct known sites on oligo- and polynucleotide polymers illustrates the widespread interest in applying fluorescence techniques for studying nucleic acid molecules (Cardullo et al., 1988; Murchie et al., 1989; Morrison et al., 1989; Cooper and Hagerman, 1990; Hochstrasser et al., 1992; Clegg et al., 1993, 1994; Eis and Millar, 1993; Parkhurst and Parkhurst, 1993; Sauer et al., 1993; Selvin and Hearst, 1994; Mergny et al., 1994). Fluorescence measurements on conjugated dye-DNA systems will undoubtedly become increasingly important for future biostructural and biotechnological applications (Clegg, 1995).

The advantages afforded by the sensitivity and specificity of fluorescence detection have long been realized in many diverse fields of nucleic acid and chromosome research. The earlier applications of fluorescence methods in nucleic acid research centered mainly around the interaction of free dye molecules with double-stranded DNA and RNA molecules (LePecq and Palotti, 1967; Löber, 1981; Dougherty and Pigram, 1982; Steiner and Kubota, 1983; Zimmer and Wähnert, 1986), and this is still an active area of research. These dyes either intercalate between neighboring bases or interact with particular chemical groups in the grooves of the helix; especially in the latter case, the interactions between the dyes and DNA often display strikingly sequence-dependent binding affinities and fluorescence properties (Zimmer and Wähnert, 1986; Loontiens et al., 1990, 1991). Much effort has been spent in determining the affinity, specificity, and structures of these DNA-dye complexes. Because the fluorescence properties of these dye molecules are often dramatically affected by their interactions with nucleic acids, the quantum yields and the polarization of fluorescence can be utilized to detect and quantify nucleic acids rapidly with samples at low concentration or with microscale quantities, as in flow cytology and fluorescence microscopy (Arndt-Jovin and Jovin, 1990; Boltz et al., 1994; Hirons et al., 1994). In addition, many studies have been carried out using these DNA-binding dyes to determine physical characteristics of the nucleic acids themselves (Bresloff and Crothers, 1975; Ryan and Crothers, 1984; Macgregor et al., 1985, 1987; Schurr et al., 1992).

We and others have used covalently attached fluorophores to study the geometry of DNA/RNA molecules in solution, especially using fluorescence resonance energy transfer (FRET) (Murchie et al., 1989; Hochstrasser et al., 1992; Clegg, 1992; Clegg et al., 1992, 1993; Gohlke et al., 1994; Selvin et al., 1994; Tuschl et al., 1994; Jares-Erijman and Jovin, 1996), and to observe the dissociation and hybridization of duplexes (Cardullo et al., 1988; Morrison et al., 1989; Clegg et al., 1993; Parkhurst and Parkhurst, 1993; Sixou et al., 1994). The main effort in these studies has been directed toward investigating thermodynamic, kinetic, and structural characteristics of various duplex DNAs, as well as of more complex nucleic acid molecules. As the sophistication of these experiments and analyses increases, it becomes necessary to determine in more detail the interactions between the dyes and the nucleic acids to which they are attached. It is difficult to determine exact molecular struc-

Received for publication 18 March 1996 and in final form 7 May 1996.
Address reprint requests to Dr. Robert M. Clegg, Max Planck Institute for Biophysical Chemistry, Department of Molecular Biology, P.O. Box 2841, D-37018 Göttingen, Germany. Tel.: 49-551-201-1-390; Fax: 49-551-201-1-467; E-mail: clegg@mpc186.mpibpc.gwdg.de.

0006-3495/96/08/972/23 $2.00

tural features of dye-DNA interactions in solution; however, if covalently attached dyes are to be used for reporting on more than only the most rudimentary characteristics of DNA/RNA structures and their conformational changes, or for quantifying these DNA/RNA structures in various environments, we must characterize the properties of these DNA-dye complexes over a broad range of solution conditions. In addition, there are often multiple molecular species present simultaneously in the solution, and we must develop measurements for distinguishing between these different species.

Dyes that are covalently attached by chemical linkers are constrained to certain domains on the nucleic acids; therefore, the effective local concentration of a dye molecule in the immediate vicinity of a particular region of the DNA molecule is extremely high. This leads to dye-DNA interactions that would not otherwise be manifested if the dye were not conjugated to the macromolecule. Many of these interactions would not play a significant role if the dye were not restricted locally on the nucleic acid. This situation is quite different from that of free dyes interacting with DNA. Dyes attached to different locations within a nucleic acid sequence encounter dissimilar molecular surroundings that may bring about disparate spectroscopic outcomes. Intimate contact between the dye molecules and specific nucleotide bases can significantly affect the observed signal. On the other hand, it is a great advantage for many applications to attach the dyes to specific sites on the nucleic acid molecule, and for this reason covalently attached fluorophores are becoming increasingly popular for many studies. Fluorophores attached to particular sites of the macromolecules report on local changes within the larger structures. If the nucleotide sequence close to the site of dye attachment is kept constant, a series of similar DNA/RNA structures can often be compared efficiently in spite of specific properties of the dye-DNA complexes (Clegg et al., 1992, 1994; Gohlke et al., 1994; Tuschl et al., 1994).

In fluorescence studies the temperature, viscosity, ionic strength, and other solvent properties are often varied to characterize the system—for instance: 1) Fluorescence quenching experiments are used to determine the exposure of a fluorescent species to a freely diffusing quencher molecule (usually electron-rich ions). 2) The dependence of fluorescence anisotropy on temperature and solvent viscosity is measured to quantify the rotational characteristics of either the dye molecules themselves or the molecules to which the fluorophores are attached. 3) Different solvent conditions (e.g., temperature, pressure, ionic strength) are varied to modify or to perturb the conformational state of a macromolecule (e.g., for measuring the thermal dissociation of a nucleic acid hybrid structure) or to affect the association of the nucleic acids with other molecules (e.g., with proteins, small molecules, or other nucleic acid components). In the course of our studies on branched and duplex DNA/RNA structures and of their conformational changes (Clegg et al., 1992; Lilley and Clegg, 1993), we have exploited especially the spectroscopic characteristics of fluorescein and carboxytetramethylrhodamine (TMRh) dyes attached to the 5′ ends of the strands of oligonucleotides. These two fluorescence probes have also been used by the majority of studies by others (Clegg, 1992; Selvin, 1995), mainly because they are readily available and are easily attached covalently to DNA, and their spectroscopic properties are well known and are convenient for many different applications (see also below). Here we report on the steady-state and time-resolved fluorescence properties of TMRh molecules covalently attached to nucleic acid structures.

In both the steady-state and the lifetime experiments, the dye-DNA complex was probed by varying the temperature and the concentration of NaCl; ethanol was titrated into the buffer to check for specific solvent effects. The text is organized as follows. First we present the steady-state fluorescence experiments because they are straightforward and these experiments provide the background for the lifetime experiments. The fluorescence lifetime measurements are then presented. In the Discussion, the model in Fig. 1 is shown to be a minimum reaction scheme compatible with the experimental results. The following information is included in the Appendix: 1) a survey of known photophysical properties of free rhodamines; 2) the simulation of steady-state fluorescence values from fluorescence lifetime data; 3) equations for describing the chemical equilibrium that we propose to account for our steady-state and lifetime results. We define the abbreviations ds as double-stranded state, ss as single-stranded state, and hp as hairpin.

MATERIALS AND METHODS

Construction of fluorescently labeled single-stranded and duplex DNA molecules

The synthesis of the labeled oligonucleotides was similar to the earlier reports (Murchie et al., 1989). Oligonucleotides that are 8, 12, 16, and 20 base pairs long were synthesized with β-cyanoethylphosphoramidite chemistry (Beaucage and Caruthers, 1981) on an Applied Biosystems 392 DNA/RNA synthesizer. In the final step of the synthesis, amino groups at the end of six-carbon linkers (Aminolink 2 from Applied Biosystems) were coupled to the 5′ ends of the DNA strands with *N*-methoxytrityl-2-aminohexyl-2-cyanoethyl-*N,N*-diisopropyl aminophosphite (Connolly, 1987). The following oligonucleotide sequences, and their complementary strands, were synthesized for the double-stranded probes: 8-mer, 5′-CCACTAGG-3′; 12-mer, 5′-CCACTGGCTAGG-3′; 16-mer, 5′-CCACTGCACTGCTAGG-3′; 20-mer, 5′-CCACTGCACTCGCTGCTAGG-3′. For experiments with single strands, an 8-mer, 5′-CCACTACC-3′, and a 16-mer, 5′-CCACTGCACTGCTACC-3′, were synthesized. These last two single-stranded probes have -CC at the 3′ end instead of -GG to avoid the formation of hairpins with duplex secondary structure (manuscript in preparation). The last step of the synthesis was done with the "DMT-on" option to facilitate reverse-phase high-performance liquid chromatography purification. Base-sensitive protection groups were removed by incubating the probes with ammonium hydroxide at 55°C for 24 h. Oligonucleotides were first purified in two steps of high-performance liquid chromatography on a Waters 600E instrument. In the first step a Waters Delta Pak C18 300 Å reverse-phase column was used with 0.1 M triethylammonium acetate and increasing amounts of acetonitrile as eluant. Collected fractions were further purified in a second step with a Pharmacia Mono Q HR 5/5 strong anionic exchange column with a quaternary amine functional group that was flushed with 10 mM NaOH (pH 12) and increasing amounts of NaCl as eluant. Collected fractions were neutralized, concentrated by evapora-

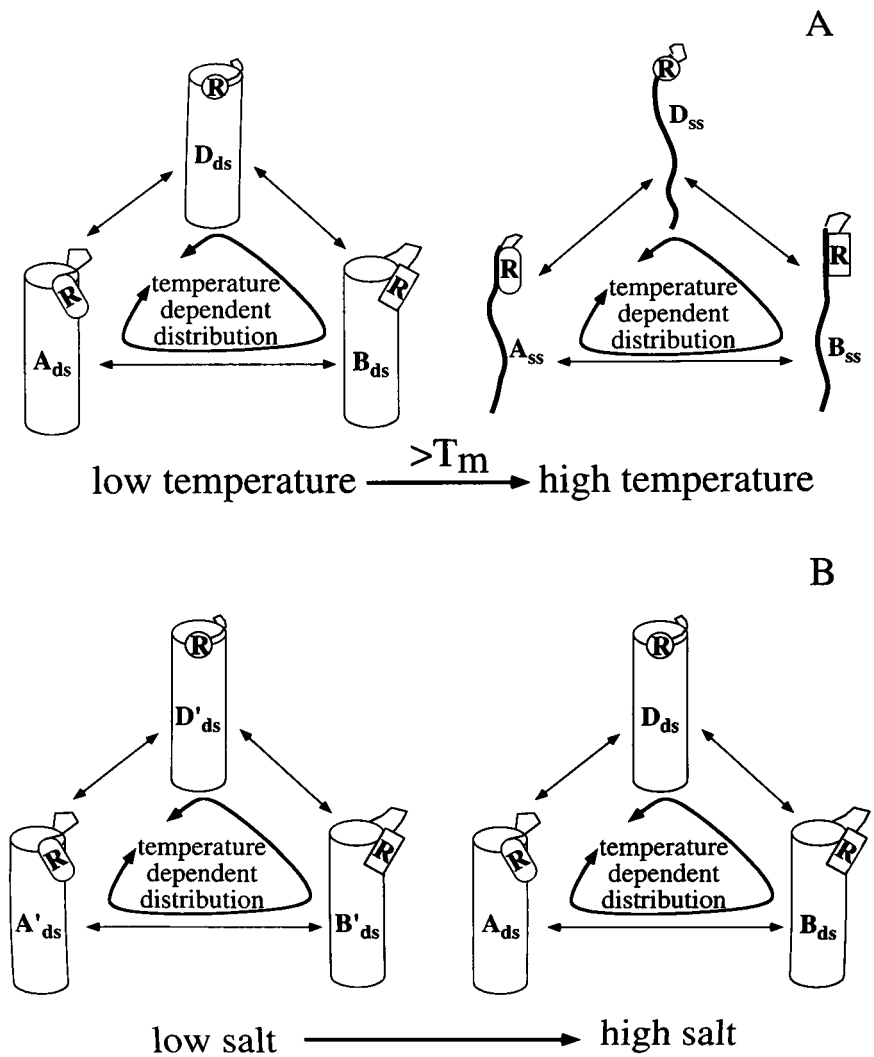

FIGURE 1 Reaction scheme of the TMRh-DNA conformers, which accounts for the steady-state and time-resolved fluorescence data. (*A*) Melting of the ds-DNA molecules when the temperature becomes greater than T_m. (*B*) Low-salt → high-salt transition. The rationalization for postulating this model is discussed throughout the text. The letters A, B, and D refer to individual molecular species (fluorescence components) of TMRh-DNA in solution (the subscripts ds and ss refer to double-stranded and single-stranded DNA molecules; in the text the ds and ss states are not explicitly indicated). A and B are fluorescent; D is a dark species of TMRh-DNA. The cylinders represent the ds-DNA molecules, and the dark narrow ribbon represents the ss-DNA strands. R is the tetramethylrhodamine chromophore that is connected to the DNA molecules by the C6 linker (thin line connecting the dye and DNA molecules). The three different patterns of the form enclosing the R symbol represent the three main species of the dye-DNA complex; these portray the three separate TMRh-DNA species. The population distribution among the separate species depends on the solution conditions; in this work, the temperature, the ion concentration, and the concentration of ethanol were varied. A, B, and D become more populated at higher NaCl concentrations; the ion titration curves can be fitted well by a simple apparent stoichiometric bimolecular binding model (see Appendix). A′, B′, and D′ are the corresponding low-salt conformations. Similar molecular species are found for both the double-stranded and single-stranded probes. Changing the temperature below the melting transition ($T < T_m$) induces the double-stranded TMRh-DNA molecules to redistribute among the different species (i.e., the relative populations of the A_{ds}, B_{ds}, and D_{ds} species depicted in *A* are temperature dependent—this is indicated by the triangular arrows *A* and *B*). The distributions among the two fluorescing species and the dark species are different at low and high salt conditions. The dark complex, D_{ds} (or D'_{ds}), is favored by higher temperatures. The shorter lifetime component, B_{ds} (or B'_{ds}), is favored over the longer lifetime component, A_{ds} (or A'_{ds}), at higher temperatures. The dominating species in the double-stranded form at higher temperature (still $T < T_m$) is the dark species (especially at higher salt concentrations; see Fig. 2 *A*). At high concentrations of salt, the dark state is much more populated than at low concentrations. For single strands we know that the shorter lifetime component is also favored by higher temperatures; however, the dark state is only a minor species for single strands.

tion, and detritylated by incubating with 80% acetic acid at room temperature for 20 min. Samples were then desalted and concentrated by Sep-Pak Light tC18 cartridges used as reverse-phase columns. Part of the synthesized oligonucleotides was selected for labeling with 5-carboxytetramethylrhodamine or fluorescein. The sequences listed explicitly above were fluorescently labeled at the 5′ amino groups with carboxytetramethylrhodamine, and their complementary sequences (for doubly labeled duplexes) were labeled with fluorescein. For the lifetime experiments the ds oligomer was always singly labeled with TMRh; the doubly labeled molecules were not used for the lifetime experiments because of possible contributions from fluorescein fluorescence. For the labeling, 0.14 mg of either 5-carboxytetramethylrhodamine succinimidyl ester or 5-carboxyfluorescein suc-

cinimidyl ester (Molecular Probes, Eugene, OR) was dissolved in 10 μl anhydrous dimethyl formamide and mixed with 30 μl of DNA oligomers (~1.7 mM strand concentration in water) and 10 μl of 1 M Na-carbonate (pH 9.5). The reaction mixtures were gently shaken for 16 h at room temperature or kept at ~35°C in a water bath. Labeled single strands were purified by polyacrylamide gel electrophoresis on 20% denaturing gels. The gel and the buffer in the tanks contained 90 mM Tris borate (pH 8.3), 0.1 mM EDTA, 7 M urea. The gel was run at ~800–1000 V, ~30 mA. The band of the labeled oligonucleotide was always well separated from the unreacted oligonucleotide. The bands were cut out of the gel, and the single-stranded oligonucleotides were extracted by electroelution. Complementary sequences were hybridized to form double-stranded molecules in 450 mM NaCl/24 mM sodium citrate/2 mM $MgCl_2$ at pH 7.0 by slow cooling from 80°C to 0°C. Double-stranded molecules were prepared with one rhodamine only, with one fluorescein only and with one fluorescein and one rhodamine at opposing ends of the duplexes. Duplex molecules were then purified by polyacrylamide gel electrophoresis on 15% native gels. The buffer contained 90 mM Tris borate, 0.1 mM EDTA, 50 mM NaCl, and 1 mM $MgCl_2$. The gel was run for ~6 h in a coldroom at ~200 V and ~60 mA. Gels were run in the dark to prevent photobleaching of the dyes. Labeled duplexes were extracted from the gel slices by electroelution or by soaking in buffer (10 mM sodium phosphate, pH 7.46, 80 mM NaCl) at 4°C for the 8-mer. Duplex molecules were dissolved and dialyzed in the same buffer to remove the salt from the electroelution. The concentration of the duplexes was determined from absorption spectra taken from 220 to 600 nm. The absorption coefficient at 256 nm used for the concentration determinations was 13,000 $M^{-1} \cdot cm^{-1}bp^{-1}$ for the double-stranded probes and 6500 $M^{-1} \cdot cm^{-1}base^{-1}$ for the single-stranded probes (Clegg et al., 1992).

The following samples were used in the different experiments presented in this paper (the concentrations are in units of duplex or single-stranded molecules): for the steady-state fluorescence temperature variation, the doubly labeled 16-mer (408 nM) and 20-mer (300 nM) duplexes (constructed with fluoresein- and TMRh-labeled strands); for the steady-state fluorescence NaCl titration, the 16-mer duplex labeled with TMRh (776 nM at 4°C, 344 nM at 16 and 27°C); for the steady-state fluorescence ethanol titration, the doubly labeled 16-mer duplex (408 nM); for the lifetime measurements with temperature variation, ethanol titration and NaCl titration: for the 16-mer and 20-mer duplexes, the 16-mer and 8-mer single strands, all labeled with TMRh and in the concentration range of 100–400 nM; for the absorption measurements with temperature variation: the 16-mer duplex labeled with TMRh (1 μM) (and the 16-mer duplex labeled with fluorescein succinimidyl ester (400 nM)).

Steady-state spectroscopy equipment

Absorption measurements were taken on a Uvicon 820 (Kontron, Z"urich, Switzerland) spectrophotometer. Steady-state fluorescence was measured with an SLM 8000S (SLM Aminco, Urbana, IL) spectrofluorimeter. Fluorescence data were corrected for fluctuations of the lamp intensity. Magic angle conditions were used to avoid polarization artifacts in fluorescence spectra. Emission spectra were corrected for the wavelength dependence of the sensitivity of the instrument. TMRh was excited at λ_{ex} = 560 nm, and the emission was measured between λ_{em} = 570 nm and 650 nm. The wavelength of excitation was λ_{ex} = 490 nm for fluorescein, and its emission was measured between λ_{em} = 500 nm and 650 nm. Steady-state fluorescence anisotropy measurements were performed at λ_{ex} = 560 nm, λ_{em} = 590 nm for probes labeled with rhodamine, and λ_{ex} = 490 nm, λ_{em} = 518 nm for probes labeled with fluorescein. Slit widths were set to 4 nm for the excitation monochromator and 2–8 nm for the emission monochromator. Fluorescence anisotropies (r) were determined from measurements of fluorescence intensities using vertical excitation polarizers with vertical ($F_{\parallel}$) and horizontal ($F_{\perp}$) emission polarizers according to $r = (F_{\parallel} - F_{\perp})/(F_{\parallel} - 2 \cdot F_{\perp})$. Polarization instrument factors were determined by using a horizontal excitation polarizer.

Steady-state fluorescence DNA melting curves

Duplex molecules were heated in steps of 4°C outside of the melting region, and 2°C in the range of the melting transition. After each newly selected temperature was reached, 10 min was allowed for chemical equilibration. The temperature was measured in a second water-jacketed cuvette in the same multisample cuvette holder with a microthermistor. Cuvettes were closed with tightly fitting stoppers to prevent evaporation.

NaCl titrations

NaCl salt titrations were carried out to determine the salt dependence of the fluorescence parameters of TMRh-DNA. Steady-state fluorescence titrations were carried out at three different temperatures (4, 16, and 27°C). Fluorescence lifetime titrations were done at 4°C. A few microliters of two different NaCl stock solutions (4.75 M NaCl, 10 mM Na-phosphate, pH 7.46; or 2 M NaCl, 10 mM Na-phosphate, pH 7.46) were added to the sample, covering a $[Na^+]$ range from 18 mM (present in the Na-phosphate buffer) to 2 M. The samples were mixed with a micro-glass rod stirrer, and then 10 min was allowed for equilibration after each addition of NaCl solution.

Ethanol titrations

For ethanol titrations, spectroscopic-grade absolute ethanol from Merck was used. Experiments were done at 18°C. During the ethanol titration, concentrated buffer and NaCl solution were titrated to the sample to retain the original buffer and salt concentrations.

Buffer solutions

For all of the spectroscopic experiments, 10 mM phosphate buffer (pH 7.46) was used with 80 mM NaCl unless otherwise indicated. The buffer was prepared by mixing Na_2HPO_4 and NaH_2PO_4. At pH 7.46, the Na^+ concentration of this phosphate buffer is 18 mM. Phosphate buffer was chosen because its pH is essentially temperature independent, $dpK_a/dT = -0.0028\ K^{-1}$ (Stoll and Blanchard, 1990).

Time-resolved fluorescence measurements

Nanosecond-lifetime measurements were carried out with the phase and modulation method (Gratton et al., 1984; Jameson et al., 1984). The instrumentation differs only slightly from that described by Piston et al. (1989), and details will be described elsewhere. The fluorescence was excited with the 514.5-nm line of a Spectra Physics argon ion laser (model 2035) and observed through a 560-nm narrow band-pass filter (560 SS, Corion, 10 nm band-pass). The orientations of the excitation and emission polarizers were set at the magic angle (54.5°) to avoid polarization artifacts. The second dynode of the photomultiplier was modulated by a frequency that equals the excitation frequency plus a 40-Hz cross-correlation frequency (heterodyne method). The current output of the photomultiplier anode was converted to a voltage, amplified, filtered at the cross-correlation frequency, and acquired with a LabPC+ DAQ card from National Instruments. The signal was integrated and fitted to a sine wave to determine phase and modulation. A standard of known lifetime (fluorescein in ethanol, 1 mM NaOH, τ = 4.13 ns; Bauman et al., 1985) was used to determine the total phase lag and the modulation of the fluorescence emission relative to the excitation light. The lifetime of the fluorescence standard was determined to be constant within the error of the measurements over the entire temperature range of the measurements. Phase and modulation data were acquired at 13 excitation frequencies ranging from 1 to 140 MHz and analyzed with a software package from Globals Unlimited (Laboratory for Fluorescence Dynamics, Urbana, IL). Mean lifetimes could be reproduced within ±0.15 ns. This was sufficient to detect lifetime differences needed to monitor the changes under investigation.

For temperature variation experiments, the temperature was increased slowly in steps of 5°C. The temperature was measured by inserting a microthermistor into a second water-jacketed cuvette filled with water. The fluorescence measurements were always performed approximately 10 min after the new temperature was reached to ensure equilibrium conditions.

Quantum yield determination of TMRh on ss, hp, and ds DNA

We determined the quantum yields (Q = ratio of the number of photons emitted to the number of photons absorbed by the fluorophore) by comparison to a dilute fluorescent standard (Demas and Crosby, 1971) of known quantum yield (rhodamine 101; Drexhage, 1973; Karstens and Kobs, 1980). The quantum yields were determined for the 5′-TMRh-labeled double-stranded 20-mer, 20-mer ss hairpin and 16-mer ss DNA molecules at 5.4°C. Emission spectra were collected in steps of 1 nm over the range λ_{em} = 555–700 nm (λ_{ex} = 545 nm) for the labeled oligonucleotide samples and for the rhodamine 101 solution. Monochromator slits were set to 4 nm for both excitation and emission. The quantum yields of the samples (Q_{sample}) were determined according to the following equation:

$$Q_{sample} = \frac{n^2_{sample}}{n^2_{Rh101}} \cdot \frac{A_{Rh101}(545)}{A_{sample}(545)} \cdot \frac{\sum_i F_{sample}(545,\lambda_i)}{\sum_i F_{Rh101}(545,\lambda_i)} \cdot Q_{Rh101}. \quad (1)$$

Q_{Rh101} is the quantum yield of Rh101, taken to be 1, and independent of the excitation wavelength in the 500–600 nm region (Drexhage, 1973; Karstens and Kobs, 1980). $A_{sample}(545)$ and $A_{Rh101}(545)$ are the absorbance values at 545 nm for the TMRh-labeled DNA and Rh101 samples. $F_{sample}(545,\lambda_i)$ and $F_{Rh101}(545,\lambda_i)$ are the fluorescence intensities measured at λ_i, excited at 545 nm. n_{sample} = 1.33 and n_{Rh101} = 1.35 are the indices of refraction for the sample (aqueous buffer, 80 mM NaCl) and of the Rh101 standard (absolute ethanol). The sums are the numerical integration over the total emission wavelengths contributing to the emission spectra.

The quantum yields of the samples are summarized in Table 1.

RESULTS

Temperature dependence of the steady-state fluorescence of TMRh on DNA

The steady-state fluorescence intensity of TMRh-DNA (λ_{ex} = 560 nm, λ_{em} = 590 nm) decreases rapidly with temperature both below (ds-DNA) and above (ss-DNA) the T_m of the oligonucleotide (see Figs. 2 *A* and 8). The dye attached to ss-DNA exhibits a greater fluorescence quantum yield than the dye on ds-DNA, as evidenced by the large increase in fluorescence intensity as the temperature passes through the ds-ss melting process of the DNA molecules (Figs. 2 *A* and 8). The peak of the emission spectrum is shifted from 588.5 to 583.2 nm as the temperature is increased from 2 to 85°C. The steady-state fluorescence anisotropy of the TMRh-DNA complex decreases with increasing tempera-

TABLE 1 Quantum yields

Sample	Quantum yield
20-mer ds	0.18
20-mer hairpin	0.40
16-mer ss	0.60

Fluorescence quantum yields of the 20-mer-ds, 20-mer hairpin, and 16-mer ss samples labeled on the 5′ end with TMRh. Details given in the text.

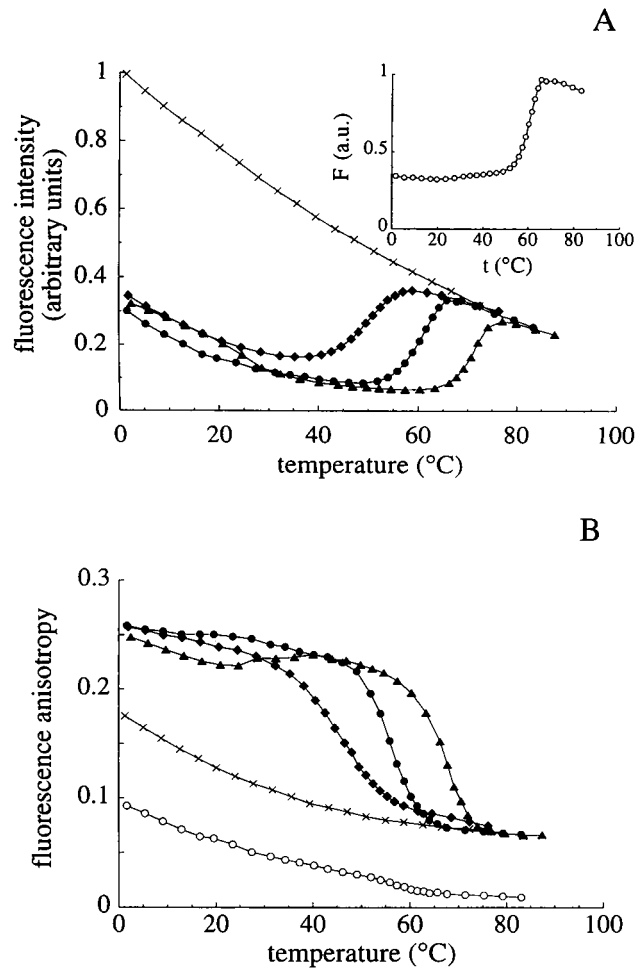

FIGURE 2 Temperature dependence of the steady-state fluorescence. (*A*) Steady-state fluorescence of TMRh on doubly labeled 12-mer (◆), 16-mer (●), and 20-mer (▲) ds oligonucleotides and singly labeled 16-mer ss oligonucleotides (×) in 10 mM Na-phosphate (pH 7.46), 80 mM NaCl as a function of temperature. λ_{ex} = 560 nm, λ_{em} = 590 nm. These curves show the melting temperature, T_m, of the duplexes at 49.3°C, 60.4°C, and 71°C for the 12-mer, the 16-mer, and the 20-mer. Below the T_m there is a dramatic decrease in the TMRh fluorescence with increasing temperature, and after the abrupt increase in fluorescence as the DNA molecules undergo their ds-ss transition, this quenching continues as the temperature is increased for the single strands. The TMRh has a higher quantum yield for single strands than for double strands. For making this plot, the intensities of the TMRh-labeled probes were matched above 80°C. For comparison, a similar fluorescence melting curve is presented in the inset for 5-fluorescein conjugated to the 5′ end of the 16-mer ds (○, λ_{ex} = 490 nm, λ_{em} = 518 nm). Of note is the very weak dependence of the fluorescein fluorescence on the temperature below the T_m of the oligomer compared to the strong temperature dependence for TMRh-DNA. (*B*) The temperature dependence of the fluorescence anisotropies, $r_{560,590}$, for the TMRh-labeled probes. The same symbols are used to distinquish the samples as for *A*. In addition, $r_{490,518}$ (○) is presented, which is the anisotropy of the fluorescein label. A dramatic decrease in the TMRh anisotropy is found at the T_m for the 12-mer, the 16-mer, and 20-mer. The prominent dip in the anisotropy of the 20-mer at ~20°C is followed by an increase in the anisotropy in the premelting region between 20°C and 40°C. This change in the anisotropy is significant and reproducible, and correlates well with the fluorescence lifetime data in Fig. 5 *A*; the α_{slow} fluorescence fraction of the slow lifetime decreases fastest between 20°C and 40°C (decreasing thereby the average lifetime), possibly leading to an slight increase in the steady-state anisotropy in this temperature range.

ture for both the ds and ss species (Fig. 2 *B*). For comparison, we have presented the temperature profile of a DNA duplex labeled with fluorescein (Fig. 2 *A*, *inset*).

The wavelength of peak absorbance of TMRh attached to DNA is also a function of temperature. The maximum is at 560 nm at 7°C, and at 555 nm at 85°C, and varies approximately linearly between. The value of the absorbance at the maximum decreases with increasing temperature in both the ds and ss regions; for ds-DNA the absorbance decreases approximately 3% from 5°C to 30°C. The ss-TMRh-DNA has a higher absorbance than the ds-TMRh-DNA; at 70°C the ss-TMRh-DNA absorbance is approximately 6% higher than for ds-TMRh-DNA. The shape of the visible absorbance melting curve is similar to that of the fluorescence melting curve shown in Fig. 2 *A*; however, the relative changes for the absorbance measurements are much less than for the fluorescence measurements (i.e., the fluorescence changes cannot be accounted for by changes in the absorbance values only).

Salt dependence of the steady-state fluorescence of TMRh on duplex DNA

Fig. 3 shows the fluorescence changes incurred by titrating with NaCl at three different temperatures below the T_m of the DNA oligomer. The fluorescence intensities decrease rapidly in the lower range of salt concentrations (up to NaCl concentrations of 0.1–0.2 M). At salt concentrations of >100–200 mM, the intensities decrease gradually as the salt concentration is increased (Fig. 3 *A*). The slow decrease in the fluorescence intensities at higher salt concentrations is assumed to be associated with a different mechanism of salt interaction than that at lower salt concentrations. The fall of the intensity curve in the higher salt regime is due mainly to dilution.

The anisotropy of the rhodamine emission (Fig. 3 *B*) increases abruptly from 0.18–0.22 to 0.24–0.27 in the initial portion of the curves where the intensities decrease; the exact values depend on the temperature of the titration experiment. The rapid change in the anisotropy values seen at lower NaCl concentrations reaches a plateau value after [NaCl] ~100–200 mM. At lower temperatures, higher NaCl concentrations are required to reach a plateau. The anisotropy values change only minimally at higher salt concentrations. The salt dependence of the fluorescence properties of the TMRh-DNA complex is a feature of the DNA complexed TMRh, not of the dye alone. Fig. 3 *C* shows the static fluorescence characteristics of free TMRh in the same buffer as the labeled oligonucleotide. The fluorescence parameters of free TMRh are insensitive to the concentration of NaCl below 0.5 M; the slight variations above 0.5 M are probably due to dynamic quenching.

Temperature dependence of the lifetime data for free TMRh

We carried out lifetime experiments with free TMRh and tetramethyl rhodamine succinimide ester (TMRh-succinim-

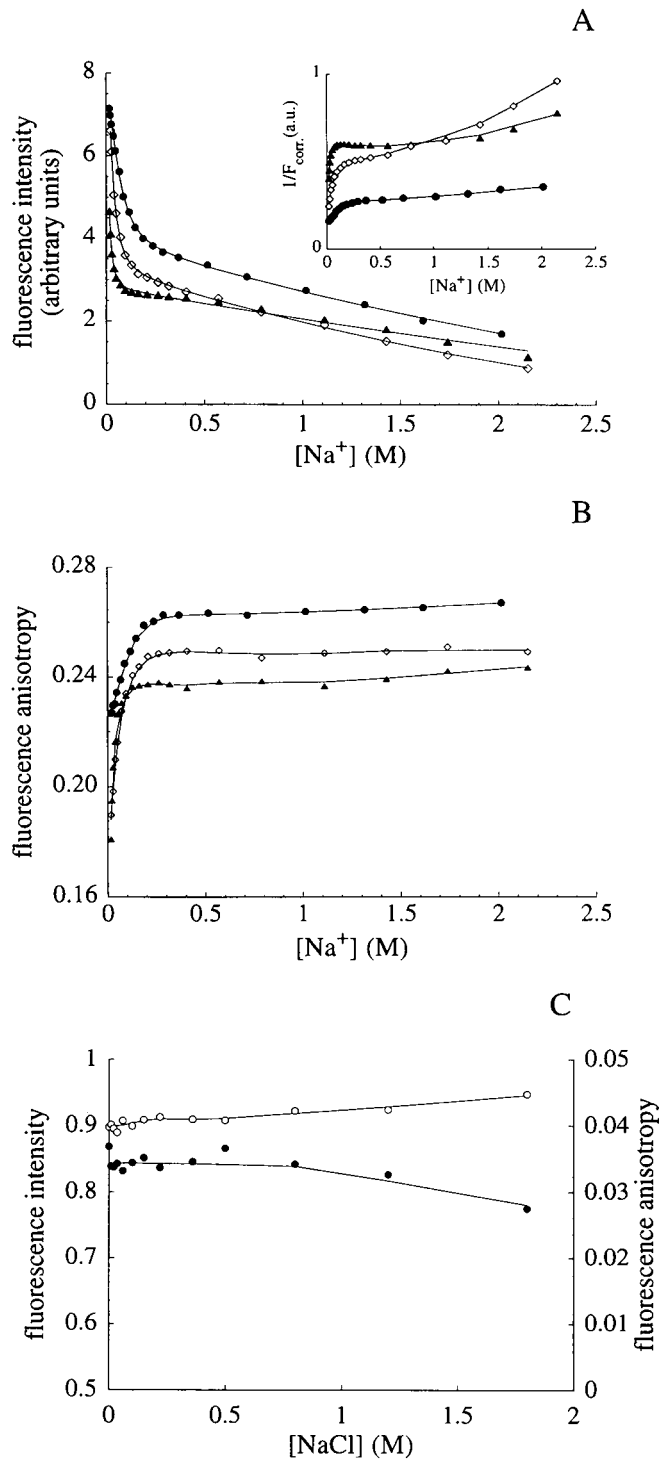

FIGURE 3 Salt dependence of the steady-state fluorescence. Dependence of the steady-state fluorescence (λ_{ex} = 560 nm and λ_{em} = 590 nm) intensity (*A*) and steady-state fluorescence anisotropy (*B*) of TMRh-DNA on the concentration of NaCl at 4°C (●), 16°C (◇), and 27°C (▲). These experiments were carried out in 10 mM Na-phosphate buffer (pH 7.46). Both the intensity and the anisotropy show a rapidly varying initial phase up to 100–200 mM NaCl, and a much more slowly varying process at higher salt concentrations. The inset in *A* is a Stern-Volmer plot of the fluorescence data. Fluorescence values were corrected for dilution in the Stern-Volmer plot. See the Discussion for an analysis and discussion of these results. (*C*) Fluorescence intensity (●) and anisotropy (○) of free TMRh in solution in the same buffer.

ide) to compare with the DNA-bound dye. Data on the temperature dependence of the lifetime of TMRh are not available in the literature (contrary to the case for rhodamine B).

The lifetime data for the free dyes can be fitted well to one exponential (in agreement with earlier measurements; Vogel et al., 1988), and the single decay time is strongly temperature dependent, as expected from the Discussion of rhodamine B in the Appendix. The temperature profiles of TMRh and TMRh-succinimide are almost identical; the TMRh fluorescence decays more rapidly by 100–200 ps throughout the entire temperature range (Fig. 4). As discussed in the Appendix, the fluorescence of free TMRh in solution decays nonradiatively only through internal conversion, and this process is dominated by an activation-controlled, temperature-dependent rate, k_{ic}. This deactivation pathway has been proposed to involve the formation of a intramolecular charge transfer (ICT) state (see Appendix for a discussion of the different hypotheses). The measured single fluorescence decay time, τ, varies from 3.4 to 1.5 ns for temperatures between 5°C and 60°C (see Fig. 4). The temperature dependence of τ can be analyzed by the expression $1/\tau = k_r + k_{iC} = k_r + k_{ic}^0 \cdot \exp(-E_a/RT)$ (Arbeloa and Rohatgi-Mukherjee, 1986; Chang and Borst, 1990); k_r is the radiative (non-temperature-dependent) rate of deactivation, E_a is an activation energy, and R is the gas constant. This analysis results in $\tau_r = k_r^{-1} = 4.85$ ns and $E_a = 6.16$ kcal/mol, with a correlation coefficient of the fit equal to 0.99959.

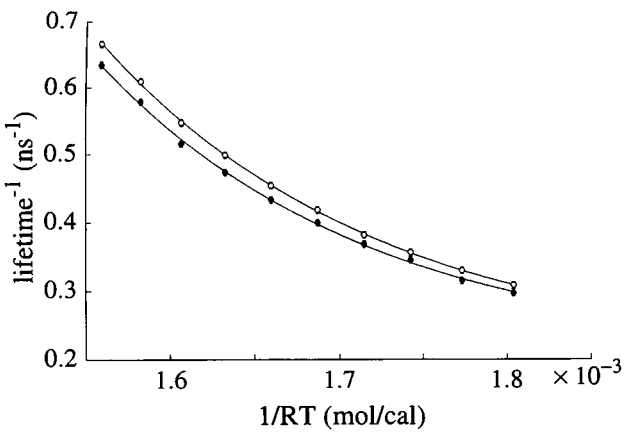

FIGURE 4 Temperature dependence of the fluorescence lifetime of the free dye. A plot of the rate of fluorescence decay (lifetime^{-1} ° τ^{-1}) versus $1/RT$, where R is the gas constant (1.986 cal · $M^{-1} \cdot K^{-1}$) and T is the absolute temperature (K) for TMRh (○) and TMRh-succinimide (●) free in solution. These experiments were carried out in 10 mM Na-phosphate buffer (pH 7.46), 80 mM NaCl. The solid lines are the result of fitting the data to the rate expressions for an activation-controlled kinetic model (see text). The strong quenching supposedly arises from the dynamic competition in the excited state between two deactivation pathways, one leading to the formation of the TICT state, and the other being the radiative fluorescence process. See text for details.

Temperature dependence of the lifetime data for TMRh conjugated to DNA

In this paper we consider almost exclusively temperature variations below the melting temperature of the DNA duplexes and for ss-DNA in the comparable temperature range. We analyze the fluorescence melting curves of these nucleic acid samples in a separate paper.

The fluorescence decay of TMRh ($\lambda_{ex} = 514.5$ nm, $\lambda_{em} = 560$ nm) conjugated to the 5′ end of ds and ss DNA was measured between 5°C and 60°C at 12 equally spaced temperatures (Fig. 5). A few of the experiments with the 20-mer duplex reported here were carried out in the absence of NaCl. The results for the time-resolved fluorescence measurements for TMRh conjugated to DNA are radically different from those for the free dye. The fluorescence of TMRh conjugated to the 5′ end of DNA oligomers decays as two distinct exponentials with time constants, τ_{slow} and τ_{fast}. A third component did not improve the χ^2 of the fit. Neither of these two lifetimes varies nearly as strongly with temperature as does the single decay time of the free dye. Similar lifetime components are found with all samples of ds- and ss-TMRh-DNA.

For ds-DNA below the melting temperature of the duplex at 80 mM NaCl, the average values of the two observed lifetimes (determined separately at each temperature) are $\tau_{fast} = 0.58 \pm 0.06$ ns and $\tau_{slow} = 3.01 \pm 0.38$ ns for the 20-mer, and $\tau_{fast} = 0.76 \pm 0.17$ ns and $\tau_{slow} = 3.06 \pm 0.4$ ns for the 16-mer (see Fig. 5 *A, open circles,* for a plot of the corresponding intensity fractions of these lifetime components). The error of each lifetime refers to the standard deviation of the lifetime from the average value determined over all temperatures. There is no obvious tendency in the dependence of the lifetimes on the temperature within the error of the measurement; therefore, the lifetimes were also linked during the fit. If the fit is carried out while linking the lifetime components separately for all temperatures (which assumes that the lifetimes are temperature independent) the fitted lifetimes over all temperatures are $\tau_{fast} = 0.57$ ns and $\tau_{slow} = 3.01$ ns for the 20-mer, and $\tau_{fast} = 0.69$ and $\tau_{slow} = 2.82$ ns for the 16-mer (see Fig. 5 *A, open squares,* for the corresponding intensity fractions). The two different fitting procedures (with and without linking) yield almost identical results for the intensity fractions of the fluorescence lifetime components, as shown for the 20-mer in Fig. 5 *A*. The inset of Fig. 5 *A* shows the fraction of the slow fluorescence component for the 16-mer, which is similar to the 20-mer below 40°C. Above this temperature the fraction of the 16-mer slow component increases; this temperature coincides with the beginning of the helix-coil transition for the 16-mer. The temperature profiles of the lifetime data for the 20-mer ds at low-salt conditions (10 mM Na-phosphate buffer, pH 7.46, no added NaCl) are presented in Fig. 5 *B*. Both lifetime components are somewhat higher than those at 80 mM NaCl. Both the increase in the slow lifetime component and the increase in the fluorescence-weighted average lifetime, $\langle\tau\rangle = \alpha_1\tau_1 + \alpha_2\tau_2$, above 50°C are coin-

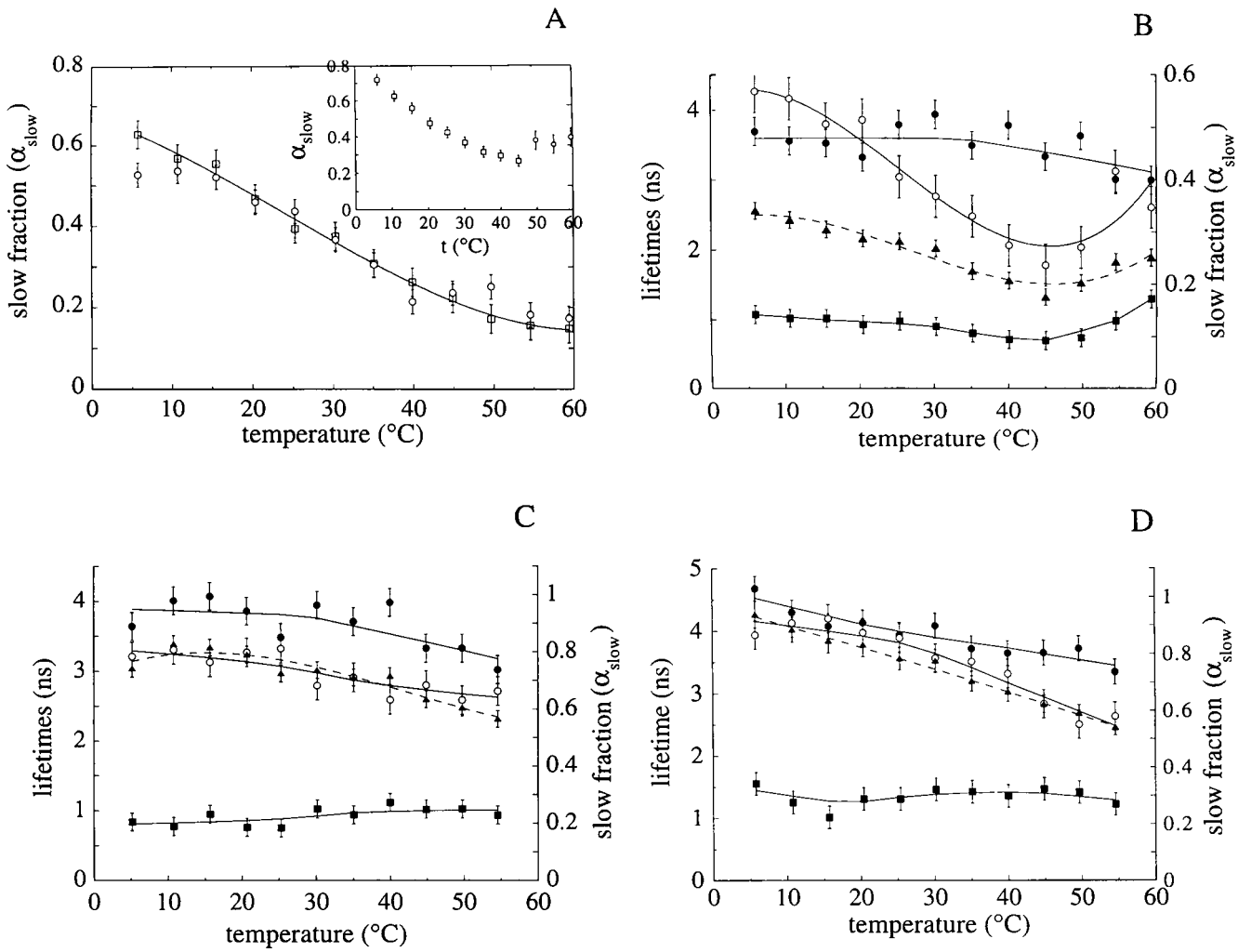

FIGURE 5 Temperature dependence of the time-resolved fluorescence parameters of the ds and ss TMRh-DNA complex. The fluorescence lifetime parameters result from fitting the fluorescence decay data to two exponentially decaying components. Notation for all graphs: α_{slow}, fluorescence intensity fraction of the slower lifetime component (○, □); τ_{fast}, lifetimes of the fast component (■); τ_{slow}, lifetimes of the slow component (●); $\langle\tau\rangle = \alpha_{fast}\tau_{fast} + \alpha_{slow}\tau_{slow}$, fluorescence-weighted average lifetimes (▲). $\alpha_{fast} + \alpha_{slow} = 1$. All samples shown in this figure are singly labeled with TMRh. The buffer contains 10 mM Na-phosphate (pH 7.46) and 80 mM NaCl except for *B*, where there is no additional NaCl present. (*A*) The 20-mer duplex. (*Inset*) The 16-mer duplex. The values of α_{slow} were obtained either by fitting two lifetime components at every temperature independently (○) or by linking the lifetimes at the different temperatures and fitting a common slow and fast lifetime component to the complete data set (□) (see the Results for an explanation and for the corresponding lifetime values). The two procedures result in almost identical values of α_{slow}. Note the increase in α_{slow} in the inset above 45°C, where the the 16-mer starts to melt. (*B*) 20-mer duplex at low salt; the beginning of the melting above 45°C is paralleled by the increase in α_{slow} and $\langle\tau\rangle$. (*C*) 16-mer single strand; (*D*) 8-mer single strand.

cident with the beginning of the helix-coil transition; the transition takes place at a lower temperature at low salt than at 80 mM NaCl.

These two separate and distinct time-resolved processes indicate the presence of at least two molecular species in solution with different fluorescence decay times. Apparently similar dye-DNA species are present below and above the T_m of the duplexes. The corresponding fractions of the total fluorescence from the two states (α_{slow} and α_{fast}) display a greater temperature variation for ds-DNA than for ss-DNA, and for ds-DNA the changes of the fractions are much larger than changes in the values of τ. For single-stranded DNA the fraction corresponding to the slowly decaying species (α_{slow}) decreases from 0.8 at 5°C to 0.65 at 60°C for the 16-mer (Fig. 5 *C*), and from 0.9 to 0.55 for the 8-mer (Fig. 5 *D*). $\tau_{slow,\ ss}$ decreases over this temperature range from 4.7 to 3.4 ns for the 8-mer, and from 3.9 to 3.0 ns for the 16-mer. The changes in the fractions for ds-DNA with increasing temperature below the T_m of the oligomers are $\alpha_{slow} = 0.55 \rightarrow 0.17$ for the 20-mer (Fig. 5 *A*) and $\alpha_{slow} = 0.65 \rightarrow 0.31$ for the 16-mer (Fig. 5 *A, inset*). The $\alpha_{slow,\ ss}$ is appreciably greater than the $\alpha_{slow,\ ds}$, especially at the higher temperatures.

Salt concentration dependence of the lifetime data for TMRh conjugated to DNA

While the fluorescence lifetimes were monitored, a salt titration was carried out at 4°C for the 20-mer over a range

of salt concentrations corresponding to the steady-state ion titrations (Fig. 6 *A*). The lifetimes and the fractional fluorescence remain almost constant over the total range of salt concentration. This shows that the fluorescing components are not quenched by the ions, and that the exchange equilibrium between the two fluorescing species (two lifetime components) is not a strong function of the ionic strength. Fig. 6 *B* is a comparison of the measured steady-state fluorescence data to the fluorescence intensity simulated from the lifetime data (see Discussion).

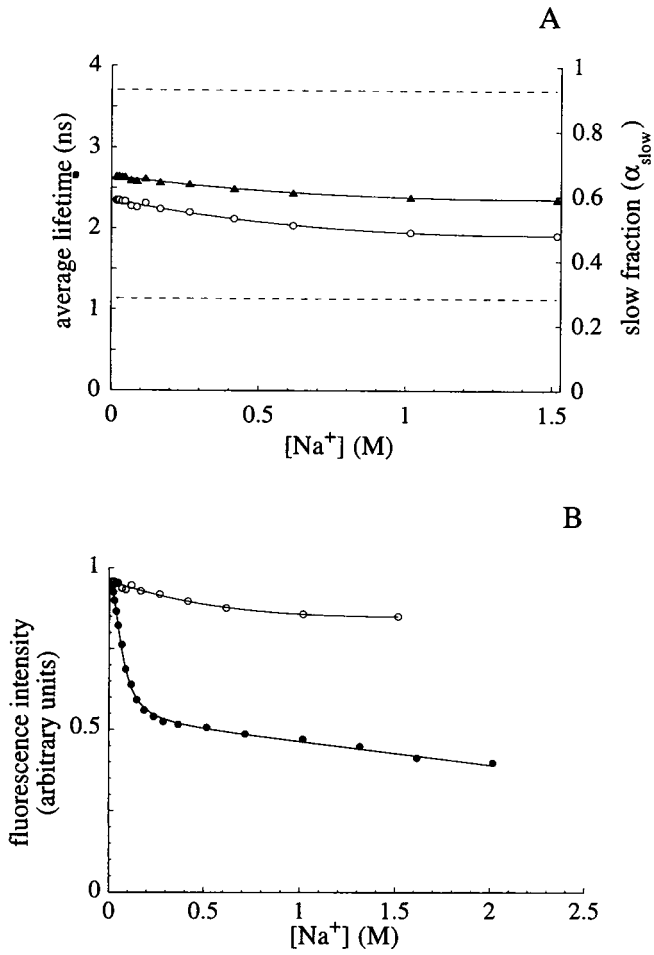

FIGURE 6 Salt dependence of the time-resolved fluorescence parameters of the ds and ss TMRh-DNA complex. (*A*) Fluorescence lifetime results of the NaCl titration of the 20-mer duplex (4°C). Fluorescence decay times τ_{fast} and τ_{slow} have been linked for all of the salt concentrations in the fit, and their values are shown as dashed lines. The fractional amplitude of the slower component, α_{slow} (○), decreases by about 18% as the concentration of the NaCl increases; the change in the lower salt regime ([NaCl] < 200 mM), where the steady state data are the most strongly affected, is not significant. ▲, Average lifetimes. (*B*) Plot showing the dependence of the measured steady-state intensity (●) on the NaCl concentration (at 4°C) and the comparison of these data to the simulated fluorescence intensity (○), assuming that only the two fluorescent species exist in solution; these latter points are calculated from the parameters of the lifetime fits (see Discussion and Appendix). The lack of congruence is direct proof of the existence of a dark state, and of the temperature dependence of the equilibrium between the fluorescing states and the dark state (see Discussion). The sample is the TMRh-labeled 20-mer duplex.

Dependence of the spectroscopic properties of TMRh-DNA on added ethanol

The polarity of the solvent can be changed by adjusting the fraction of ethanol in the buffer. The effect of ethanol on the spectral characteristics of TMRh-DNA for the 16-mer and 20-mer duplexes was observed by absorption, steady-state fluorescence intensity and anisotropy measurements, and lifetime determinations. In each experiment ethanol was added to the sample to a final concentration of 16% w/w. During the course of the titration the steady-state fluorescence intensity increases by ~40% (see Fig. 7 *A*) and the absorption coefficient increases by ~15% (data not shown); the maximum of the emission spectrum shifts from 588.5 to 585 nm and the absorption maximum shifts slightly, from 559.8 to 557.8 nm (data not shown). The fluorescence intensity does not reach a plateau value, but to avoid large perturbations of the DNA structure we did not titrate further. The lifetime experiments show that the equilibrium between the two fluorescent states does not change considerably; ~50% of the fluorescence intensity is derived from the τ_{slow} state (Fig. 7 *C*). The mean lifetime changes only slightly over this concentration range of EtOH (Fig. 7 *C*). The change in the steady-state fluorescence anisotropy (Fig. 7 *B*) is consistent with the behavior of the lifetimes.

DISCUSSION

General reaction scheme for TMRh-DNA interactions

The results can be interpreted well by the reaction scheme summarized in Fig. 1; this reaction scheme is compatible with all of the steady-state and lifetime fluorescence experiments presented below. The letters A, B, A′, and B′ refer to fluorescent dye-DNA species, and D and D′ are nonfluorescent or "dark" species of the dye-DNA complex. The primes designate low-salt forms, and the unprimed species designate higher salt forms (≥100 mM NaCl). The primed and unprimed molecular species are in equilibrium with each other through a salt-binding reaction (S stands for salt; in this work, salt = NaCl). The justification for proposing this reaction model is presented in the following Discussion sections. The steady-state fluorescence measurements alone show that there must be more than a single species of the TMRh-DNA complex. From the fluorescence lifetime data we can derive quantitative estimates for some of the thermodynamic and spectroscopic properties of these separate conformational species.

Steady-state studies

Temperature dependence of the steady-state fluorescence measurements

One of the most dramatic features of the fluorescence of rhodamine-labeled DNA is the decrease in the fluorescence intensity below and above the melting temperature of the

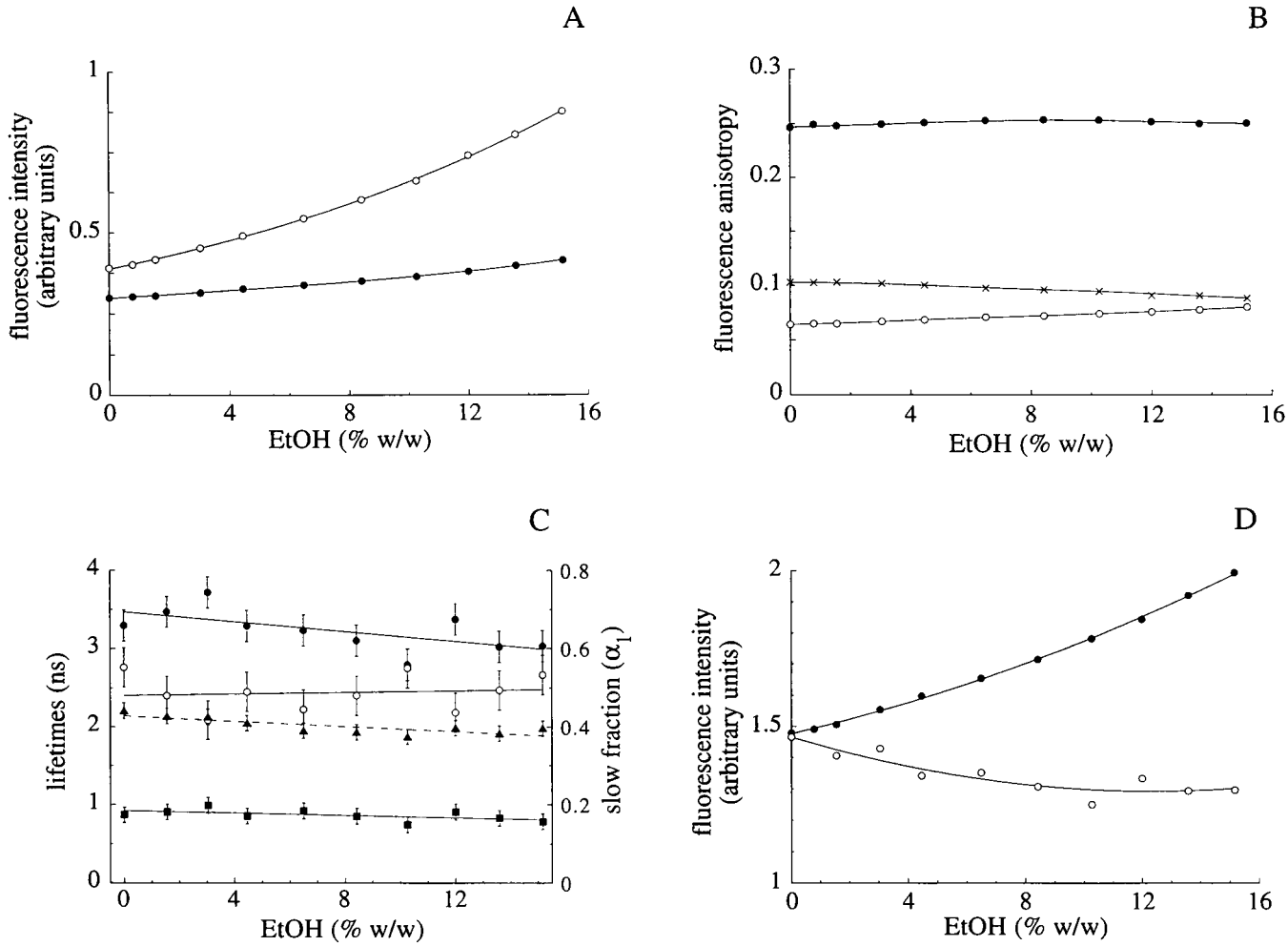

FIGURE 7 Dependence of the fluorescence parameters upon added ethanol. Presentation of the steady-state and time-resolved fluorescence data for fluorescein-DNA and TMRh-DNA at different ethanol concentrations. Measurements were carried out at 18°C. The fluorescence of fluorescein and rhodamine from doubly labeled probes can be separated; exciting at 490 nm, only the fluorescence of the fluorescein is detected around 518 nm; only the rhodamine is excited at 560 nm. (*A*) Fluorescence intensity of TMRh fluorescence (●, λ_{ex} = 560 nm, λ_{em} = 590 nm) and of fluorescein fluorescence (○, λ_{ex} = 490 nm, λ_{em} = 518 nm) of doubly labeled 16-mer duplexes (80 mM NaCl). The fluorescein data are given as a comparison to the TMRh data; fluorescence resonance energy transfer (FRET) affects this fluorescein signal (see *B*). (*B*) Steady-state fluorescence anisotropy measurements of the doubly labeled 16-mer with different excitation and emission wavelengths: λ_{ex} = 560 nm, λ_{em} = 590 nm (●; rhodamine fluorescence alone), λ_{ex} = 490 nm, λ_{em} = 518 nm (○; fluorescein fluorescence alone) and λ_{ex} = 490 nm, λ_{em} = 590 nm (×; this is a mixed fluorescence measurement, exciting mainly the fluorescein donor and observing the fluorescence emission of mainly the rhodamine acceptor; this measurement is very sensitive to the efficiency of FRET). (*C*) Plot of the τ_{fast} (■) and τ_{slow} (●) fluorescence lifetimes, the fluorescence fraction of the slow component α_{slow} (○) and the mean (weighted by the fluorescence intensities) lifetime (▲) of TMRh versus ethanol concentration, for the 20-mer singly labeled duplex. (*D*) Plot comparing the dependence of the measured steady-state fluorescence intensity (corrected for changes in the absorption) of 16-mer TMRh-DNA duplex (●) on the ethanol concentration to the simulated fluorescence intensity of the singly labeled 20-mer duplex, assuming that only the two fluorescent species exist in solution (○); these latter points are calculated from the parameters from the lifetime fits (see Discussion and Appendix). This is direct evidence that the increase in TMRh fluorescence as the ethanol concentration is increased is due to a decrease in the population of the dark-state species.

DNA; the melting process is accompanied by a large increase in the fluorescence intensity as the DNA probes pass from the double-stranded to the single-stranded state (see Fig. 2 *A* and 8, *A* and *B*). This difference in the fluorescence intensity of rhodamine-labeled double-stranded and single-stranded DNA oligomers is a useful spectroscopic characteristic that can be used to distinguish the duplex from the single-stranded state in, e.g., DNA hybridization studies. However, the large decrease in the fluorescence intensity above and below the melting region (see Figs. 2 *A* and 8) makes it more difficult to extract thermodynamic information from these melting curves. In addition, the decrease in the fluorescence of the double-stranded state is not linear; e.g., the fluorescence decreases more rapidly at lower temperatures and tends to level out between 30 and 60°C.

There is an abrupt change in the anisotropy in the temperature region including the T_m of the oligonucleotide. At temperatures outside of the melting processes, the anisotropy values decrease only slowly (Fig. 2 *B*). A decreasing fluorescence anisotropy in spite of large decreases in fluo-

rescence intensities is an indication that the decrease in the fluorescence intensity is not due to dynamic quenching. Two processes play a dominant role in determining the fluorescence anisotropy, and they act in opposing directions as the temperature is increased: 1) increasing the rate of rotational diffusion of the dye (e.g., by increasing the thermal motion of the dye and lowering the viscosity) will decrease the value of anisotropy, and 2) increasing the rate of dynamic quenching (again due to a decreasing viscosity) will decrease the fluorescence lifetime, leading to higher anisotropy values. Originally we tried to simulate the weak temperature dependence of the anisotropy by assuming that the large decrease in the fluorescence intensity was due to dynamic quenching (which would substantially decrease the fluorescence lifetime) and by simulating the temperature dependence of the rotational diffusion of the dye molecules with different models. We were not able to simulate the steady-state data with reasonable models including only these two temperature-dependent processes. To account for the large decrease in the fluorescence intensities of the duplex molecules by dynamic quenching, the decrease in the fluorescence lifetime would become so extreme that rotational diffusion alone could not induce the observed anisotropy decrease.

This led us to carry out fluorescence lifetime experiments, which eventually showed that there are two observed lifetime components and that the fluorescence lifetimes do not change significantly over the range of temperature variation. Therefore, there is no evidence of strong dynamic quenching; on the other hand, as the temperature is increased, the population of the shorter lifetime component increases at the expense of the slow lifetime component (see Discussion below). In addition, increasing the salt concentration promotes the transition to the A and B states from the A′ and B′ states (Fig. 1), and this produces an increase in the fluorescence anisotropy (Fig. 3 *B*); this salt effect is very temperature dependent (Fig. 3 *A*). The model of a temperature- and salt-dependent transition between the multiple states (Fig. 1) that we propose to use to interpret the fluorescence lifetime experiments, together with the expected decrease in anisotropy due to increasing rotational diffusion, is compatible with the gradual temperature-dependent, steady-state anisotropy changes seen in Fig. 2 *B*.

The model of Fig. 1 accounts for both our steady-state and lifetime fluorescence results, and involves essentially static quenching processes. (In this work we refer to the quenching of a fluorescent species as static not only if it is a true static quenching (e.g., the formation of a nonfluorescent ground-state complex, or where the rate of fluorescence is drastically reduced), but also if there is an extremely rapid and efficient dynamic quenching process that is too rapid for our lifetime detection apparatus.) As discussed below, we assign the temperature dependence of the fluorescence of the labeled molecules outside of their melting region mainly to a temperature-dependent redistribution of the DNA-bound rhodamine molecules among the three states (i.e., a chemical reaction with species A, B, and D) discussed in Fig. 1. According to this model, the rapid decrease in the static fluorescence intensity with increasing temperature is partially due to the formation of a dark species of the TMRh-DNA (D). In addition, there is a gradual redistribution between the fluorescent species (A and B) with increasing temperature that decreases the population of the slower lifetime component and increases the population of the faster lifetime component. The apparent quenching of the fluorescence is not simply related to the relative diffusion of the bound fluorophore and a quencher.

The absorbance of TMRh attached to DNA slightly decreases as the temperature is increased (by ~3% between 5–30°C in the ds form; data not shown). The population of the dark state (D and D′ of Fig. 1) increases and the populations of the fluorescing states (A, A′, B and B′ of Fig. 1) decrease over this temperature range (see discussion below). This might be an indication that the absorption of the dark state is less than that of the fluorescing states. In this respect, it is interesting to note that the π-electron system of the TMRh dye is interrupted upon formation of the lactone, and this drastically changes the chromophoric properties compared to those of the nonesterified acid form (Drexhage, 1973).

The NaCl titrations monitored by static fluorescence measurements reveal a strong interaction of monovalent ions with the labeled DNA to form a TMRh-DNA-ion complex

We have previously noted that the anisotropy of Rh-DNA samples is sensitive to the salt concentration (Clegg et al., 1992), and this provided the initial impetus for studying the salt dependence of the interaction between conjugated TMRh and DNA. To gain a global description of the interaction between TMRh and DNA brought about by the increase in the concentration of NaCl, we treat the titration curve as an approximate two-state binding process between the salt and the TMRh-DNA. The early part of the salt titrations, up to ~100–200 mM NaCl, can be fitted to an apparent simple bimolecular binding model after correcting for the gradual fluorescence intensity decrease at high salt with a linear function. We assume that Na^+ is the interacting ion:

$$n \cdot [Na^+] + [\text{TMRh-DNA}] \leftrightarrow [Na^+\text{-TMRh-DNA}]_{\text{complex}}. \quad (2)$$

n refers to the number of Na^+ ions bound. The model refers only to the interaction of the salt with the TMRh-DNA complex; we are not inferring that Na^+ binds in general stoichiometrically to the polyelectrolyte structure of the DNA. The titration data were fitted to this model by expressing the fluorescence intensity in terms of the concentrations and minimizing the variance of the difference between the data and the fit using a nonlinear regression technique (the fit was carried out within the framework of the program IGOR Pro; WaveMetrics, Lake Oswego, OR). The effect of the dilution on the intensity is taken into account in the fitting procedure. The data fit quite well

quantitatively to this simple model. We show in the Appendix that the more extended binding model of Fig. 1 can exhibit the same overall binding behavior as the simple binding model in Eq. 2. The solid lines in Fig. 3 *A* are the fits of the data to the model of Eq. 2; the results of such fits are given in Table 2. The number of ions (n) and the equilibrium constant at each temperature are both independent variables in the fitting procedure.

It is seen already from the raw titration data that the interaction of salt is an endothermic process and that the heat absorbed upon binding must be large. The resulting apparent equilibrium constant at different temperatures can be analyzed further by a van't Hoff plot, giving an apparent enthalpy change of $\Delta H^\circ = +29$ kcal/mol for the binding of salt to the DNA/dye structure. Even considering the phenomenological nature of this enthalpy change, this is a peculiar value of ΔH° for a simple binding reaction of salt; it is endothermic and quite large. The accompanying apparent entropy change is large and positive for the binding reaction ($\Delta S^\circ = 110$ cal/(mol · K)). This positive entropy change suggests that the contribution of hydrophobic forces to the overall interaction of the dye to the DNA may increase as the interaction of salt with the dye-DNA complex increases. Such hydrophobic interactions probably occur at the surface of TMRh molecules, and as a result the rotational mobility of the dye molecule would be reduced, leading to an increase in its anisotropy, as is observed (Fig. 3 *B*). The loss of water surrounding charges upon their interaction could contribute significantly to the enthalpy change. We emphasize that these ΔH° and ΔS° values cannot be assigned to elementary reaction steps. These apparent ΔH° and ΔS° values should be considered cautiously; they indicate only overall tendencies of the ion-dye-DNA complex formation and do not refer to an individual reaction step.

Large abrupt changes in the extent of interaction between singly charged ions and the polyelectrolyte DNA are not expected in the concentration range of 10–200 mM NaCl (Manning, 1979; Soumpasis et al., 1990; Record et al., 1978). Nevertheless, the salt titration data of Fig. 3 imply a specific stoichiometric interaction between the three reaction partners—DNA, ions, and dye. At pH 7.46 TMRh is expected to exist as a zwitterion with a partial positive charge on the amino groups and a partial negative charge on the carboxyl group; perhaps the ions participate as a "bridge" between the DNA and the DNA-conjugated dye. When the changes in the fluorescence intensities at lower salt concentrations are analyzed with a Stern-Volmer plot (Birks, 1975) (this would assume that the decrease in the fluorescence is due to dynamic quenching), the resultant apparent diffusion constants ($D = 2.2 \cdot 10^{-3}$, $7.1 \cdot 10^{-3}$, $7.4 \cdot 10^{-3}$ cm^2/s at 4°C, 16°C, 27°C) are far too large to correspond to a reasonable molecular diffusion process. The diffusion constants of Cl^- (the probable quenchers if the quenching is dynamic) for these temperatures are estimated from the Stokes equation to be much smaller: $D_{est} = 0.73 \cdot 10^{-5}$, $1.05 \cdot 10^{-5}$, $1.43 \cdot 10^{-5}$ cm^2/s at 4°C, 16°C, 27°C. This illustrates that the pronounced ion-induced quenching is not associated primarily with a simple dynamic quenching mechanism that would be coupled directly to the diffusion of ions in solution. This conclusion agrees with the weak dependence of the observed lifetimes on the ion concentration (Fig. 6). Apparently the TMRh molecules attached to DNA are partially protected from direct interactions with the ions that are diffusing in the solution. In contrast with these data for TMRh-DNA, the quenching of fluorescein-DNA fluorescence can be accounted for by a simple Stern-Volmer mechanism at NaCl concentrations between 20 mM and 1500 mM (Clegg et al., 1992).

A plot of $1/F$ versus [NaCl] (Stern-Volmer plot) for [NaCl] > 100 mM shows a nonlinear positive deviation (see Fig. 3 *A, inset*). Such a deviation cannot be due to a singular quenching event; and at NaCl concentrations greater than 0.3 M, the salt interaction effective at lower concentrations is essentially complete. The interaction between the DNA bases is expected to become tighter as the salt concentration is increased (e.g., a reduced electrostatic repulsion between the phosphate charges is associated with increased T_m values). This could weaken the interaction between the dye and the DNA bases, thereby altering the quenching interactions and possibly allowing more interaction of the dye with the salt ions in the solution. The anisotropy of the TMRh actually increases slightly in this high salt range, possibly because of the slow decrease of the faster fluorescence lifetime at higher salt concentrations.

It is clear from the above steady-state fluorescence data that there are probably more than one species of dye-DNA complex present at any time in solution. To investigate this in more detail we have carried out fluorescence lifetime experiments.

TABLE 2 Apparent ion association constants to TMRh-DNA

T (°C)	K_a (M^{-2})	n
4.7	231	2.06
16	983	2.00
27.2	9160	2.00

The fit parameters of the NaCl titration curve according to the reaction in Eq. 1. K_a is the association constant, and n is the number of ions binding to one molecule of the TMRh-DNA complex.

Lifetime studies

In the Appendix we have summarized the literature on time-resolved fluorescence studies of rhodamine dye molecules free in solution. The reader who is unacquainted with this work may find it helpful to refer to this material as background before proceeding to the following discussion. The apparent spectroscopic response of the TMRh-DNA molecule to environmental changes, and its observed lifetime decay spectrum are quite different from those found for the free dyes in pure solvents. The spectroscopic properties of TMRh are modulated by interactions with the DNA molecule, and there are separate multiple species of TMRh-DNA with distinct spectroscopic characteristics.

The two observed lifetimes are direct evidence that at least two species of TMRh-DNA are present simultaneously. These two lifetime components are always observed, as well as a dark species (the dark state may only be a very minor species for ss-DNA; see Fig. 8, *C* and *D*); therefore, we have specified in our general reaction model in Fig. 1 that there is a set of two fluorescent species and one dark state for both ds- and ss-DNA; these three molecular species are present at high salt (>100 mM NaCl) and a corresponding (perhaps identical) set of three molecular species at lower salt. The values of the lifetimes of the two fluorescing species depend only weakly on the temperature (Fig. 5) and on the salt concentration (Fig. 6).

The fluorescence decay of the free dyes, TMRh and TMRh-succinimide, are single exponential, and the temperature dependence is consistent with a thermally activated deactivation process

The value of E_a (6.16 kcal/mol) compares well with literature values measured for rhodamine B by others. The apparent E_a for RhB was first determined by Karstens and Kobs (1980) to be 6.6 kcal/mol in ethanol (see also Ferguson and Mau, 1973, and Snare et al., 1982). It has been found (Chang and Borst, 1990) that E_a for RhB is a function of the polarity of the solvent, but not of the viscosity; this indicates that the rotation around the amine bond is not controlled by viscosity-limited random diffusion. We have

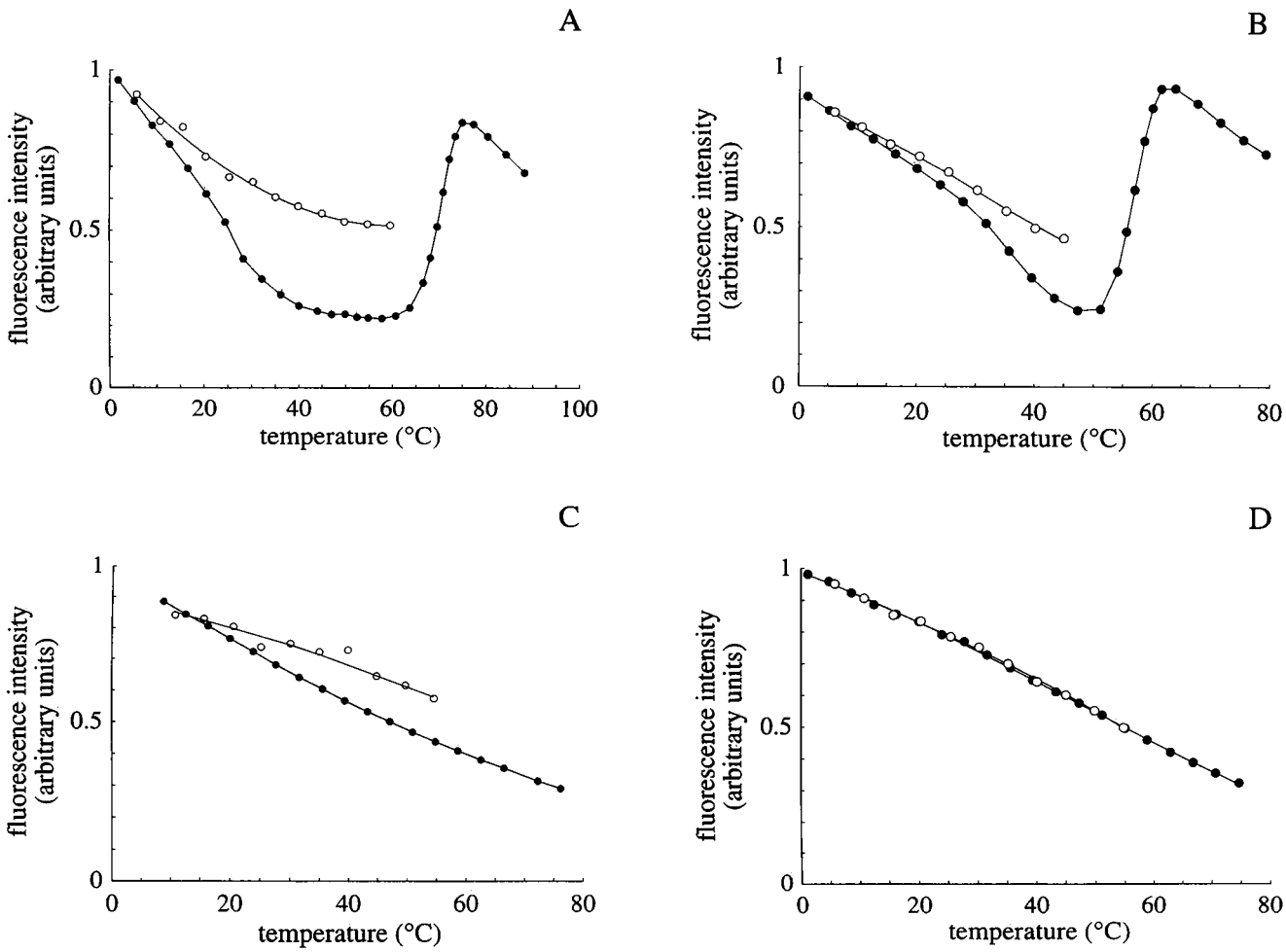

FIGURE 8 Comparison of the temperature dependence of the measured steady-state fluorescence intensity of ds and ss TMRh-DNA to that of the fluorescence intensity simulated from lifetime data. The measured temperature profiles of the steady-state fluorescence intensity (●) of TMRh-DNA are compared to the simulated steady-state intensities calculated from the lifetime parameters (○), assuming that only the two fluorescent species (i.e., no dark state) exist in solution. This simulation is explained in the Appendix. A comparison of the shape of these two curves is a strong indication of a dark state of TMRh-DNA (see text). In the plot, the two curves are arbitrarily set equal at the lowest temperature, where the population of the dark state is minimal. All samples are in 10 mM Na-phosphate buffer (pH 7.46). (*A*) The 20-mer duplex at 80 mM NaCl and (*B*) at no added NaCl; (*C*) the 16-mer and (*D*) the 8-mer single strands, both at 80 mM NaCl. The lack of congruence between the measured and calculated curves in *A* and *B* is direct evidence of the existence of a dark state, and the temperature dependence of the equilibria between the fluorescing and dark species. The decrease in the lifetimes and the exchange between the slow and fast lifetime components seems to explain the temperature dependence of the fluorescence intensity of the 8-mer single-stranded probe. The approximate congruence in the case of the 16-mer ss (*C*) and the perfect coincidence for the 8-mer imply that there is either no dark state of the single-stranded TMRh-DNA complex or its amount is not largely affected by temperature.

not been able to find a value for the apparent E_a for the carboxyl form of TMRh in the literature, but it is expected to be similar to that for RhB. It has been reported that the E_a of the ethyl ester of TMRh is 15% less than the E_a for the ethyl ester for RhB (Vogel et al., 1988). We emphasize again that the presence of multiple fluorescent components and the temperature dependence of the TMRh-DNA fluorescence contrast strongly with the fluorescence characteristics of free TMRh in solution (Fig. 4 and Appendix).

The expected steady-state fluorescence intensity of TMRh-DNA can be calculated from the fluorescence lifetimes and their amplitudes

This comparison between the lifetime and steady-state fluorescence results (for both the temperature variation experiments and salt titrations) reveals direct evidence for the dark state, as we show in the following sections. It is possible to calculate the expected steady-state fluorescence intensity of a sample from the lifetime data if the fluorescence decay of every fluorescence component in the solution can be observed (see Appendix). If the two fluorescent species (A and B in Fig. 1) belonging to the two observed lifetimes (Fig. 5) were the only two molecular species present in solution (i.e., if no dark species were present; this is equivalent to the absence of species D and D′ in Fig. 1), one should be able to account for the temperature (or salt) dependence of the steady-state temperature (or salt titration) curves by calculating the steady-state fluorescence intensity from the lifetime data. This steady-state fluorescence intensity that is calculated from the lifetime data ($F^{\text{calc from }\tau}_{\text{steady-state}}$) can be compared with the measured steady-state fluorescence (Fig. 3 *A*) over the temperature (or salt) range of the experiments. The normalized coefficients of the fluorescence lifetime components resulting from fitting frequency domain lifetime data ($\alpha = a_i \cdot \tau_i$; see Materials and Methods, the Appendix, and definition of static quenching, above) are the actual fractional contributions of the different fluorescent species to the steady-state (time-integrated) static fluorescence signal (Lakowicz, 1983; Jameson et al., 1984). If we make the assumption that the quantum yield of each fluorescent species is proportional to its lifetime, then the steady-state amplitude calculated from our observed lifetime parameters is (see Appendix for a short derivation, Eq. A4)

$$F^{\text{calc from }\tau}_{\text{steady-state}} = N_{A+B} \cdot \left(\frac{1}{\tau_r}\right)\{a \cdot \tau_f^A + b \cdot \tau_f^B\} \propto Amp \cdot \{a \cdot \tau_f^A + b \cdot \tau_f^B\}. \quad (3)$$

a and b are the fractions of molecules in the two states A and B, and it is assumed here that $a + b = 1$ (that is, it is assumed for this calculation that A and B are the only two species of TMRh-DNA in the solution). τ_f^A and τ_f^B are the fluorescence lifetimes of species A and B, N_{A+B} is the total number of molecules excited per unit time, and τ_r is the radiative lifetime (assumed to be the same for the TMRh in both the A and the B species; see Appendix). *Amp* is a normalization coefficient, the value of which is chosen to match the two fluorescence intensity scales of the lifetime and the steady-state fluorescence experiments; it contains the corrections for the exciting light intensity, absorption coefficients, concentrations, photomultiplier sensitivities, etc. We are only interested in the form of the fluorescence versus temperature (or salt) curve, so the quantity *Amp* is an arbitrary constant and is used only to normalize (at one temperature or salt concentration) the intensity derived from the time-resolved fluorescence data to the measured steady-state intensity. We can see from Figs. 6 *B*, 7 *D*, and 8 that, except for the 8-mer single strands (Fig. 8 *D*), we are unable to account for the static fluorescence data from the information in the lifetime data alone.

The discrepancy between the measured and calculated steady-state intensities for ds-TMRh-DNA results from the fact that N_{A+B} in Eq. 3 does not represent the total number of rhodamine molecules. Because of the equilibrium between the fluorescing species (A and B) and the dark species (D) shown in Fig. 1, N_{A+B} is, in actuality, not constant for the set of temperature (or salt concentration) data (as was assumed in the calculations of $F^{\text{calc from }\tau}_{\text{steady-state}}$). If N_{A+B} varies with the temperature (or NaCl concentration), the change in $F^{\text{calc from }\tau}_{\text{steady-state}}$ results not only from $\{a \cdot \tau_f^A + b \cdot \tau_f^B\}$, as was assumed in the simulation, but also from the temperature (or salt)-dependent value of N_{A+B}.

Two separate fluorescent states and a dark state of the TMRh-DNA are disclosed by measuring the lifetimes during the salt titrations

The two fluorescence lifetimes and the fractional contributions of the two lifetime components changed only very little (Fig. 6) over the range of salt concentrations where the fluorescence intensity and anisotropy show the most pronounced changes. Therefore, the relative fractions of the two fluorescent species are apparently not a strong function of the salt concentration, and the exchange between only these two fluorescent species cannot explain the strong decrease in the observed fluorescence intensity of the steady-state ion titrations in Fig. 3. Fig. 6 *B* shows a comparison of the salt dependence of the measured steady-state fluorescence of the 16-mer with the expected steady-state fluorescence calculated from the data of Fig. 6 *A*, assuming that the only species of the TMRh-DNA in solution are the two fluorescent species (see Appendix and discussion above). The lack of congruence between the data and this calculation is direct evidence for a dark state of TMRh-DNA (species D′ and D of Fig. 1).

In addition, because the lifetimes vary only a little (especially for the double-stranded species), the substantial increase in the fluorescence anisotropy that accompanies the increase in the salt concentration from 10 to 100 mM (see Fig. 3) is due to a decrease in the rotational mobility of the TMRh dye. It was shown in the previous section that the

interaction of NaCl with the TMRh-DNA complex is highly endothermic, and there must be major rearrangements of the contributing molecular groups of the DNA and the dye. A stiffening of the molecular environment of the dye upon ion binding is probably the cause of the anisotropy increase upon the addition of salt; i.e., the dye is held more rigidly at higher salt conditions. Nevertheless, although the enthalpy and entropy differences between the conformations of A′ and B′ at low salt, and between A and B at higher salt (see schematic in Fig. 1) are large—which indicates a rather drastic molecular rearrangement of the DNA—the equilibrium constants between the two fluorescent forms at low (A′↔B′) and high (A↔B) salt are not significantly affected by salt. The transition between the two fluorescent species and the dark-state species does not take place within the lifetime of the excited state because the fluorescence lifetimes remain essentially constant for all of the NaCl concentrations, despite the large change in the steady-state intensity. If the decrease in the quantum yield were due to an increase in the rate of nonradiative deactivation from the excited state, we would observe a shortening of the fluorescence lifetimes.

If the dark state were the only species at higher salt concentrations, the fluorescence would become completely quenched during the titration. This is not the case, and it is direct evidence that the salt also interacts with the two fluorescent TMRh-DNA species. The two fluorescent TMRh-DNA species at lower and higher salt seem to be the same (or very similar) molecular species, because their fluorescence lifetimes remain constant throughout the salt titration. The addition of salt modulates the relative distribution between the two species, but not their fluorescence lifetimes.

Van't Hoff analysis of the equilibrium between the two fluorescing species that can be resolved by lifetime measurements

The lifetime studies show that the fractional occupancy of the two fluorescing states is dependent on the temperature; the fraction of the slow lifetime decreases with increasing temperature in both ds and ss probes (Fig. 5). The time-resolved fluorescence components can be related to molecular species at different temperatures if the assumption is made that the quantum yields of the two molecular species corresponding to the slow and fast fluorescence components are proportional to their fluorescence lifetimes. This is equivalent to assuming that the two emitting TMRh-DNA species have the same fundamental molecular spectroscopic properties. That is, the two molecular species are assumed to have the same radiative rate k_r. The two species have different lifetimes because they experience different environments and have different rates of nonradiative deactivation.

The temperature dependence of the relative fraction of the slow fluorescence component ($\alpha_{slow,\ ds}$) for the 20-mer oligomer at 80 mM NaCl (Fig. 5 *A*) and with no added salt (Fig. 5 *B*) can be analyzed as a conformational change. To do this the fluorescence intensity fractions, α, must be converted to fractions of molecules, a; the latter are proportional to the number of molecules. (The conversion between these two component fractions is $a_k = (\alpha_k/\tau_k)/[\Sigma_i(\alpha_i/\tau_i)]$, and $\alpha_k = a_k \cdot \tau_k/\Sigma_i a_i \cdot \tau_i$.) A monomolecular van't Hoff analysis of these data results in the following thermodynamic parameters: for ds-DNA $\Delta H° = +8.3$ kcal/mol and $\Delta S° = +32$ cal/mol/K (the $\Delta H°$ and $\Delta S°$ for conditions of no added NaCl are identical); for the 8-mer ss-DNA $\Delta H° = +8.4$ kcal/mol and $\Delta S° = +27$ cal/mol/K. These values are calculated for increasing temperature, that is, for the transition from the slow lifetime state to the fast lifetime state. These two thermodynamic values are similar to the $\Delta H°$ and $\Delta S°$ expected to unstack an average base pair positioned internally in a DNA helix ($\Delta H° \approx +8$ kcal/mol and $\Delta S° \approx 24$ cal/mol/K) (Breslauer et al., 1986).

There is a prevalent dip in the TMRh-DNA anisotropy-temperature curve for the 20-mer (Fig. 2 *B*). The anisotropy curves are very reproducible and the amplitude of the dip is far outside the error of the anisotropy measurement. The physical source of the dip in the fluorescence anisotropy curve of the 20-mer can be explained by observing (in Fig. 5 *A*) the temperature dependence of the A→B transition from the τ_{slow} component (A in Fig. 1) to the component (B in Fig. 1). Initially the anisotropy decreases slowly, probably because of an increased rate of rotation of the TMRh molecule as the temperature is raised. However, the population of the TMRh-DNA molecules is continually shifting (with increasing temperature) from the τ_{slow} to the τ_{fast} state (Fig. 5 *A*), and the mean fluorescence lifetime is thereby decreasing. The τ_{fast} state has a higher anisotropy due to its faster fluorescence decay, and eventually this state becomes the dominant fluorescent component. As the τ_{fast} state becomes populated, the measured anisotropy increases slightly, and when the transition is over, the anisotropy continues its gradual decrease with increasing temperature. It is interesting that the A→B transition also leads to an increased Förster resonance energy transfer, as can be seen by the small decrease in the fluorescein fluorescence intensity in this temperature range for the doubly labeled molecules (see Fig. 2 *A, inset*). Unpublished data, obtained from the FRET from fluorescein to TMRh by observing the normalized sensitized increase in the acceptor (TMRh) fluorescence, also show this increase in the FRET efficiency even more dramatically (manuscript in preparation). The A→B transition can also be seen in the shape of the fluorescence intensity curve (Fig. 2 *A*) in the temperature range of 10–30°C. Similar behavior of the fluorescence intensity and anisotropy curves can also be observed for the 16-mer, but to a lesser extent. The observation of these processes supports our proposed model in Fig. 1 involving the A→B transition between two well-defined states of TMRh-DNA.

The free energy difference between the τ_{slow} and τ_{fast} components appears to be very similar for the double- and single-stranded TMRh-DNA molecules. This indicates that the interaction between the TMRh and ds-DNA is not due to

structural entities that are specific for double-stranded DNA, such as interactions in the groove. It is more likely that the TMRh is interacting with the faces of the bases, and possibly directly with the phosphates (see below).

The value of τ_{slow} for the ss-TMRh-DNA molecules approaches the estimated radiative lifetime τ_r of TMRh at low temperatures (τ_r was estimated to be 4.85 ns from our measurements with TMRh in Fig. 4). Thus the quantum yield for the slow fluorescence component at low temperatures is almost unity; this indicates that the rotation around the amine bond may be almost completely hindered for the TMRh molecules in this species.

Further confirmation of a dark state is obtained by simulating the expected steady-state fluorescence temperature and salt titration profiles from lifetime data

A simulation of the temperature profiles of the steady-state fluorescence intensity using the lifetime data (analogously to the simulation for the titration data) and its comparison to measured steady-state data (Fig. 1 *A*) gives a further indication of the existence of the dark-state species of the TMRh-DNA complex. Fig. 8 *A* shows the result of such a comparison for the 20-mer at 80 mM NaCl. A similar curve with less pronounced deviations is found for the 20-mer at low salt (Fig. 8 *B*). Comparing the steady-state measured data with the expected steady-state fluorescence intensity simulated from the time-resolved data shows that the temperature-dependent changes in the fractional occupancy of the two fluorescent states observed in the lifetime experiments cannot account for the profile of the measured temperature-dependent steady-state fluorescence intensity curve for ds-TMRh-DNA molecules. We observe only two lifetime components, and there is no measurable indication of faster fluorescence components; therefore, we conclude that a dark state (i.e., a molecular dye-DNA species with a very low, or zero, quantum yield; D′ and D in Fig. 1) must be populated to a significant extent in the solution in addition to the two observable fluorescing species, and that the population of the dark state increases with increasing temperature.

The presence of the dark state is not so pronounced for the ss-TMRh-DNA samples, as can be seen by comparing the $F_{\text{steady-state}}^{\text{calc from } \tau}$ simulated values with the measured steady-state fluorescence intensities in Fig. 8, *C* and *D*. As a matter of fact, the $F_{\text{steady-state}}^{\text{calc from } \tau}$ values account quite well for the ss-TMRh-DNA data, especially for the 8-mer ss-TMRh-DNA sample. This indicates either that the dark state is only a minor component in the ss-DNA state, or that there is no temperature-dependent redistribution between the A and B states with the D state for ss-TMRh-DNA molecules.

A dark state is also indicated by the ethanol titrations monitored by steady-state and time-resolved fluorescence

The 40% increase in the steady-state fluorescence intensity upon the addition of ethanol (Fig. 7) cannot be accounted for by changes in the extinction coefficient (which changes maximally by 15%), by changes in the lifetimes, or by changes in the distribution between the two fluorescing species. Fig. 7 *D* shows the comparison of the measured fluorescence intensity versus [EtOH] with the expected steady-state fluorescence calculated from the lifetime data in Fig. 7, assuming that only the two fluorescent species are present in the solution (see Eq. 3). In contrast to the measured increase in the fluorescence intensity, the calculated steady-state intensity actually decreases if the assumption is made that only the fluorescent species, A and B, exist. This discrepancy implies the presence of a nonfluorescent dark state (D of Fig. 1) that is in equilibrium with the two discernible fluorescent species (A and B of Fig. 1), in agreement with the temperature variation and salt titration experiments above. The fraction of TMRh-DNA molecules in this dark state decreases upon the addition of ethanol. The fact that the fluorescence intensity increase (Fig. 7 *A*) is accompanied by constant fluorescence lifetimes as the ethanol concentration is increased is evidence that the transition to the dark species does not take place within the lifetime of the excited state. Otherwise we would expect the fluorescence lifetimes to lengthen as the ethanol concentration increases. This, together with similar results for the NaCl titration, is further evidence that the distribution among the A, B, and D species is a ground-state distribution.

Ethanol favors the dissolution of molecular aggregates or complexes with partial nonpolar character, and renders nonpolar molecules more soluble in an aqueous environment. The effect of ethanol in our experiments is to decrease the free energy of stabilization of the dark state relative to the fluorescent A and B states, thereby decreasing the population of the dark state. From this point of view, the dark state of TMRh-DNA would be expected to be less polar than fluorescent states A and B. There are large enthalpic and entropic contributions involved in the transition from the dark to the fluorescent states of TMRh-DNA, and this may be due to conformational changes in the DNA structure at the end of the helix associated in the transition from the dark state to the fluorescent states. However, it is unlikely that the ethanol induces a transition to single-stranded DNA, because the anisotropy does not change over the entire ethanol range. Whatever the reason for the increase in the fluorescence intensity in the presence of ethanol, the fluorophore still remains in close interaction with the DNA; apparently, according to the lifetime results, the fluorescent states of the TMRh-DNA molecules are the same A and B states as in the absence of ethanol.

The quantum yield of fluorescein (see Fig. 7 *A*) and the absorption coefficient of rhodamine are both increased by the addition of ethanol. This leads to an increase in the efficiency of Förster resonance energy transfer between the two dyes, which are on opposite ends of the doubly labeled DNA duplex. This in turn decreases the fluorescence lifetime of fluorescein, leading to an increase in its fluorescence anisotropy (Fig. 7 *B*, open circles). The decreasing anisot-

ropy of the "mixed" experiment (observing both fluorescein and rhodamine fluorescence) is also indicative of increasing FRET efficiency as the concentration of ethanol is increased (Fig. 7 *B*, ×) (Clegg et al., 1994). The independence of the TMRh anisotropy (filled circles) is a reflection of the constant lifetimes and fractional amplitudes shown in Fig. 7 *B*.

An overall reaction model for interpreting the data

We have proposed the model shown in Fig. 1 as an explanation of the steady-state and lifetime-resolved fluorescence data for TMRh-DNA. Because the values of the two separate lifetimes are only weakly dependent on the temperature and on the salt or ethanol concentrations, a dynamic quenching process does not play a significant role within the time window of the fluorescence decay from the excited state of the DNA-conjugated TMRh. Such an activation-controlled dynamic process takes place with free TMRh, where the fluorescence lifetime is strongly dependent on the temperature and a kinetic process after excitation results in a nonfluorescent molecular species (see Fig. 4 and Appendix). The mechanism for forming a dark state for the free dye is often attributed to the rotational freedom of the dialkylamine-xanthene bond or an amino nitrogen inversion (see Appendix).

In stark contrast to the case of the free dye, the geometrical rearrangement of the dimethylamine group around the amine-xanthene bond is apparently hindered by the interaction of the TMRh with the DNA, at least for the two fluorescing states A and B (A′ and B′ at low salt) in Fig. 1. The lifetimes of the two fluorescent TMRh-DNA species show only a weak temperature dependence (Fig. 5). The absence of a pathway for deactivation directly from the initial excited state to a dark state for those fluorescent components that are observed would lead to only a weak temperature dependence of the rate of fluorescence decay. Note that this does not mean that the dark state of the TMRh-DNA is not similar to the nonemitting state for the free dye (see next paragraph). It only means that the two fluorescent states and the dark state are derived from separate ground-state species and do not interconvert within the excited-state lifetime. In this regard it is interesting that the fluorescence lifetimes and the quantum yields of free TMRh and RhB molecules in highly viscous solutions, in glasses, or at low temperatures are independent of temperature (Karstens and Kobs, 1980; Vogel et al., 1988); under these conditions the rates of formation of the presumed TMRh or RhB nonfluorescent states are slower than the radiative lifetime. In addition, for conditions of low temperature or high viscosity, two fluorescence lifetimes have been observed for RhB with values similar to our values for TMRh-DNA (Bergamasco et al., 1990). The two fluorescence lifetimes are direct evidence of (at least) two emitting species.

On the other hand, for TMRh-DNA the rate of formation of the nonemitting dark species must be much faster than the natural rate of emission; therefore, for TMRh molecules in this state, the dark species is always produced. It is reported for the free rhodamine dyes that for larger twist angles around the alkylamine-xanthene bond (found for increasing sizes of the alkyl groups), the transition to a nonfluorescent state takes place faster (Rettig, 1986; Vogel et al., 1988). If the plane of the amine group is twisted away from coplanarity with the xanthene ring system and the twist angle is large enough, the fluorescence is essentially completely quenched; that is, the lifetime of the excited state is greatly reduced. This may well be true for the dark state of TMRh-DNA. As a working model, we propose that in one of the TMRh-DNA species (the dark state that is most stable at high salt and higher temperature) there is a relatively strong interaction of the amine groups with the DNA leading to a larger twist angle than is normal for the free TMRh in solution. If this bond is already twisted sufficiently in the ground state, the rate of the transition to a nonfluorescent state after excitation would be much more rapid than the radiative rate, and this would be indistinguishable from a statically quenched ground-state dark species.

Possible TMRh-DNA interactions

What are the DNA-dye interactions responsible for the formation of three molecular species of TMRh-DNA that have such different fluorescence properties? Although any proposition concerning the relative spatial orientations and interactions between the dye molecules and the DNA must remain purely speculative at the moment, we may try to correlate our results with the known solvent effects on the free dye. We do not expect that the dye-DNA interactions are specific to the helical state of DNA, because the steady-state and lifetime-resolved spectroscopic parameters are very similar for the ss- and ds-DNAs. The specific interactions of the dye molecules with the DNA may be similar to the specific solvent effects discussed above for the free dye (see Appendix). The charged chemical groups of TMRh —the dimethylamine groups and the carboxyphenol group—probably interact with the salt ions, the water, and the phosphates of the DNA backbone. In addition, it is quite likely that the flat xanthene ring system would prefer to stack on a molecular surface (e.g., of the nucleotides) if the electrostatic forces are compatible with this mode of binding. It is known that free TMRh in solution forms dimers and higher aggregates that are nonfluorescent. It has been proposed that these dye-dye aggregates involve TMRh molecules that are stacked face to face (Drexhage, 1973; Kemnitz et al., 1986). The mutual stacking of dye molecules does not pertain to our experiments, because only a single dye molecule is conjugated to each DNA oligomer and the concentrations are very low. The large positive apparent ΔH° resulting from the analysis of the salt titrations is an indication that a cooperative change in the structure of the DNA may be involved when the salt binds; the ΔH° value corresponds to the magnitude of ΔH° for the opening of two or three base pairs at the end of the DNA helix. There may

be a rearrangement of the base pair structure at the end of the DNA molecule that involves dye-nucleotide interactions; this interaction is strengthened by adding ions. The positive apparent $\Delta S°$ is further indication of dye-nucleotide interactions (possible hydrophobic interactions).

Implications for using TMRh as a reporter dye on nucleic acids

Besides the discovery of two emitting TMRh-DNA states, a major finding of this study is the existence of a dark state, that is, a TMRh-DNA species that does not fluoresce. All of these states behave as separate ground-state species that do not interconvert within the lifetime of the two fluorescent excited states. The population of the dark state accounts for most of the fluorescence quenching effected by increasing temperature and by the addition of NaCl. The fractional occupancy of the two fluorescent states is also temperature dependent, and their quantum yields are different (probably proportional to the lifetimes); however, the temperature dependence of the equilibrium between these two states accounts for only a fraction of the quenching of the steady-state fluorescence as the temperature is raised. The equilibrium between the fluorescent states is only weakly dependent on the NaCl concentration. The complexity of TMRh-DNA spectroscopy, which is closely related to the sensitivity of the dye to its molecular surroundings and to the environmental conditions, makes it a very useful probe for following conformational changes such as the melting of duplexes.

The existence of multiple conformations of TMRh molecules linked to DNA with different quantum yields (one state having a quantum yield of approximately zero) must be taken into account in any detailed analysis of fluorescence properties of TMRh-labeled DNA. For instance, the meaning of the parameters that result from fitting lifetime-resolved FRET measurements to doubly labeled DNA molecules (Eis and Millar, 1993; Hochstrasser et al., 1992) with a relatively complex physical model that involves a continuous spatial distribution of the dye molecules must be examined more carefully. Furthermore, quantifying the amount of DNA labeled with TMRh with fluorescence measurements should be approached with caution because the effective quantum yield may even vary with the solvent conditions and with the position of labeling. The existence of more than one orientation of the absorption transition dipole of TMRh with respect to the DNA molecule can affect the interpretation of fluorescence anisotropy decay curves and FRET measurements. Obviously the interpretation of anisotropy decay of the TMRh-DNA complex depends not only on the relative orientation of the dye molecules to the DNA, but also on the presence of multiple dye orientations. On the other hand, multiple orientations of transition dipoles usually increase the probability that FRET measurements may be interpreted with a constant orientation factor (κ^2) close to the value of 2/3 (Haas and Katchalski-Katzir, 1978; Clegg, 1996); this is especially true if the distance between the donor and acceptor is greater than the critical distance (R_0) for energy transfer (Wu and Brand, 1992). In this respect, it is an advantage for FRET measurements that TMRh molecules have multiple orientations; however, it is probably not expedient to assume a particular unique orientation of the TMRh molecule relative to the DNA when interpreting FRET data on TMRh-labeled nucleic acid molecules. FRET efficiencies should be determined in more than one way (e.g., from donor fluorescence quenching, acceptor fluorescence enhancement, donor and acceptor "mixed" anisotropies, and fluorescence lifetimes; Clegg, 1992). Caution is advisable when comparing values of the efficiency of FRET from measurements of the donor fluorescence with efficiency values from the normalized acceptor fluorescence if TMRh is used as an acceptor; the dark state acts as an acceptor in the former case, but the transfer to the dark state would not be observable in the latter case. In this sense determining FRET efficiencies from measuring donor (e.g., fluorescein) fluorescence is more complex than making the complementary determination from the acceptor (TMRh) fluorescence (Clegg, 1992). To check for such problems, we have made extensive determinations of FRET efficiencies with various methods (Clegg et al., 1992; Gohlke et al., 1994) and have usually found good agreement between them, especially at lower temperatures. This indicates that the different fluorescent species of TMRh are located in similar locations on the DNA molecules, at least for the molecules we have studied. The absorption coefficients of the different states of TMRh-DNA are fairly similar (see above); however, the fluorescence parameters are very different and the fractional occupation of the different states depends on the solution conditions and possibly on the nucleic acid sequence. These effects would be difficult to correct for when measuring FRET by the extent of steady-state donor quenching; it is therefore not advisable to use TMRh-DNA as a donor in FRET experiments.

CONCLUSIONS

We have identified multiple species of TMRh molecules that are conjugated to the 5′ end of DNA. Three discrete, well-defined states of TMRh-DNA can been discriminated by their differential steady-state and lifetime-resolved spectroscopic characteristics; the relative population of the TMRh molecules among the three different species is dependent on the temperature and solvent conditions. The interaction of the salt (NaCl) with the TMRh-DNA complexes is over and above that expected for ion-polyelectrolyte effects. The $\Delta H°$ and $\Delta S°$ values for the salt interaction are large and positive; this may be an indication that the interaction of ions with the TMRh-DNA complex is associated with a combination of cooperative rearrangement of part of the DNA structure, water rearrangements around the participating electrical charges, and hydrophobic effects. We have also carried out titrations of free TMRh with DNA (data not shown); the concentration of DNA required for an

observable interaction is in the millimolar range, and the spectroscopic changes in the free dye upon interaction with DNA molecules are very different from those described for the DNA-dye complexes above (data not shown). The particular interactions and spectroscopic properties discussed above apply specifically to the case in which the dye molecule is covalently conjugated to the 5′ end of the DNA via a C_6 linker. It is likely that the fluorescence properties of TMRh linked to DNA depend on the sequence of bases near the end of the DNA; this would be especially pronounced for single-stranded DNA.

We have studied the spectroscopy and physical interactions of TMRh that is covalently linked to DNA molecules in more detail than has been reported previously in the literature for this or other DNA-linked dyes. Such studies are crucial if more sophisticated applications of fluorescently labeled nucleic acid molecules are to be reliably performed, such as more refined fluorescence-based sequencing procedures and detailed stereochemical determinations of nucleic acid structures. The photophysical response of TMRh-DNA is qualitatively quite different from free TMRh in pure solvents. Similar behavior can be expected for many organic dyes attached covalently to nucleic acids. This does not hinder the application of such covalently attached fluorescent labels (even in the absence of such detailed photophysical studies) for a variety of quantitative measurements, such as monitoring the binding of proteins to DNA, carrying out FRET measurements, and determining the dynamic anisotropy decay of labeled nucleic acid structures in different environments. However, once the fluorescence parameters of the dye-DNA complexes have been determined, the quantitative interpretations of these measurements can be refined.

APPENDIX

Spectroscopy of rhodamine dyes

There is a long history of research dealing with the spectroscopic properties of xanthene dyes (starting with the synthesis by von Baeyer of fluorescein in 1871 (Römpp and Raaf, 1982) and, soon after, of rhodamine). These dyes, and their derivatives, have been employed for a variety of purposes probably more than any other fluorophores, and there have been numerous studies of their physical spectroscopic properties. The popularity of fluorescein in biochemical and chemical analyses is due to its high absorption coefficient, high quantum yield, low toxicity, and the fact that the emission is within the wavelength region of the visible spectrum where the eye is most sensitive (Voss, 1984). Rhodamines also form a family of related structures with high absorption coefficients, high quantum yields, and exceptional stability that makes them attractive for applications requiring high sensitivity and resistance to photolysis. Xanthenes have been extensively investigated for use as laser dyes (Drexhage, 1973) and form the chromophoric group for a new set of calcium probes (Haugland, 1992). Earlier, only a mixture of 5- and 6-substituted isomeric labeling reagents was available for labeling amine and sulfhydryl groups; however, it is now possible to synthesize separately the 5- and 6-substituted labeling reagents (Corrie and Craik, 1994), and these are now also commercially available (in this work we use 5-carboxytetramethylrhodamine succinimidyl ester for labeling).

The spectral characteristics of rhodamines depend strongly on the different chemical structures attached to the amino groups and to the phenyl group. Rhodamines with electron donor and acceptor moieties attached to the xanthene ring are especially sensitive to the polarity and chemical nature of the solvent. The dialkylamino substitutions are particularly sensitive to temperature variations as well as to the polarity of the solvent. The photophysics of rhodamine B (tetraethylrhodamine) has been studied in detail. Despite many investigations, there is no universally accepted model representing the luminescence decay of rhodamine B and related rhodamines; however, several of the working hypotheses have some common elements. Some spectroscopic characteristics of rhodamines that pertain to our rhodamine-DNA studies are reviewed in the following paragraphs. This Appendix is meant to provide an introduction to the vast literature of rhodamine photophysics. The reader must keep in mind that there is still a lively discussion in this field concerning the interpretation of the mechanism of luminescence of dialkylamino rhodamines and related compounds, and there is no consensus of opinion at the moment.

The quantum yield of dialkylamino rhodamines

The rate of intersystem crossing for rhodamines is slow ($k_{isc} \approx 10^7\ s^{-1}$; Penzkofer and Falkenstein, 1978; Arbeloa et al., 1989). Therefore, the main nonradiative deactivation process is due to internal conversion. The transition moment of the main absorption band (450–600 nm) is oriented parallel to the long axis of the xanthene ring system (Kuhn, 1959). Some of the transitions of the shorter wavelengths are oriented perpendicular to the long axis (Jakobi and Kuhn, 1962). Rhodamines can exhibit very high quantum yields ($\phi \approx 1$; Drexhage, 1973; Karstens and Kobs, 1980); however, it has been known for a long time that the quantum yields of some rhodamines, especially the dialkylamino rhodamines, are very sensitive to the temperature, to the polar and hydrogen-bonding characteristics of the solvent, and to the viscosity (Förster and Hoffmann, 1971; Snare et al., 1982).

The following is a short review of the prominent models of the photophysical characteristics of rhodamine dyes.

The TICT hypothesis

The extreme sensitivity of dialkylamino rhodamines (for instance, tetramethyl- and tetraethylrhodamine) to temperature and solvent parameters has been attributed to peculiarities of the dialkylamino groups. Upon excitation, the initial locally excited (LE) state forms an intramolecular charge transfer state—the LE-ICT state; in this state the amino group partially donates an electron to the xanthene ring system, which serves as an electron charge acceptor. If the conjugation between these two moieties in the molecule is retained (that is, the amino bond has at least a partial double bond character through resonance with the xanthene ring), there is only a differential charge separation within the molecule. It was suggested early (Förster, 1951) that the amino substituents could become twisted in the excited state, rotating away from their initial planar orientation to the xanthene ring system. This rotational isomerization has been interpreted by Grabowski et al. (1979) to form a twisted intramolecular charge transfer (TICT) state (Grabowski et al., 1979; Rettig, 1986) (this state has never been observed directly for rhodamines because it does not fluoresce (Vogel et al., 1988), in contrast to the TICT state of some other fluorophores). By twisting out of the plane of the xanthene ring, the resonance conjugation between the ring system and the amino moiety is broken and the amino link acquires single-bond character; this has the effect that the charge in the TICT state is transferred completely from the amino group to the xanthene ring system, leading to a very large dipole moment in the molecule. As long as the molecule is in this twisted state, there is no possibility for decreasing the charge separation, as would be possible if the charge separation could equilibrate through a resonance double bond between the rings and the amino group. The electron donor and acceptor groups are assumed to be uncoupled in the TICT state (the "principle of minimal overlap"; Grabowski et al., 1979).

The proposed TICT state in rhodamines has been investigated in detail. The geometrical arrangement of the amine group relative to the xanthene ring (assumed in the TICT hypothesis to be related to the freedom of

rotation around the bond joining the amine group to the xanthene ring) has been shown to play a central role by comparing the temperature dependence of the fluorescence quantum yield and the lifetime for rhodamine B (which has diethylamino moieties attached to the xanthene ring) with that of rhodamine 101 (which has a rigid double bridge structure holding the amine group rigidly in place; Karstens and Kobs, 1980). By comparing many different *N*-substituted rhodamine dyes, it has been demonstrated that electronic and steric factors affect the rate of nonradiative inactivation from the excited state (Vogel et al., 1988). The energy of a TICT state (E_{TICT}) can be related to the ionization potential of the electron donor (*IP*(D), for rhodamines the amine group), the electron affinity of the acceptor (*E*(A), for rhodamines the xanthene ring), the coulomb attraction between the separated charges (*C*), and the stabilization energy of the solvent (ΔE_{solv}): $E_{TICT} = IP(D) - E(A) + C + \Delta E_{solv}$ (Grabowski et al., 1979; Rettig, 1986). If the groups attached to the nitrogens have too low a capacity for donating an electron and the ΔE_{solv} is not sufficient, E_{TICT} will be large compared to the energy of the initial locally excited state, E_{LE}, and the TICT state will not be populated. For many molecules that form a TICT state, dual fluorescence is observed to originate both from the LE and the TICT states; the proposed TICT state of rhodamines does not fluoresce. As this energy difference between these two states, $E_{TICT} - E_{LE}$, becomes smaller, the rate of formation of the TICT state increases, thereby decreasing the quantum yield and lifetime of the LE-ICT state. The rate does not appear to be controlled by a viscosity-dependent stochastic rotation (Chang and Borst, 1990). For rhodamines the lack of emission from the TICT state is attributed either to a rapid internal conversion from the TICT excited state (in the picosecond time range) or to the lack of orbital overlap for the transition dipole matrix element between the TICT state and the ground state, together with insufficient vibrational coupling between these two perpendicular states, to make the electronically nonallowed transition possible. The fluorescence of tetraethylrhodamine decays slightly more rapidly than that of tetramethylrhodamine, and the temperature sensitivity of the rhodamine B fluorescence is more pronounced (Vogel et al., 1988). This has been proposed to be a consequence of the larger torsion angle in the ground state between the planes of the amino group and the xanthene ring system for rhodamine B (Drexhage, 1973). This initial twist for the diethylamino group, compared to the dimethylamino group, increases the rate of formation of the twisted state upon excitation. The formation of the TICT state is the major nonradiative pathway for deactivating the locally excited state (LE) of rhodamines, and this is the major temperature-dependent rate of deactivation. According to this interpretation, the decrease in the fluorescence lifetime and the accompanying quantum yield decrease with increasing temperature of tetramethyl- (and tetraethyl-) rhodamine are due to the increasing rate of formation of the twisted molecular conformation. The activation energy for TICT formation depends on the substituents attached to the nitrogen; for dimethylamino rhodamine in ethanol it is reported to be 26.5 kcal/mol (Vogel et al., 1988).

Arguments against TICT states

The hypothesis of TICT states has recently been challenged (Zachariasse et al., 1993; von der Haar et al., 1995); because these arguments are based on experiments with compounds that have been central to the TICT hypothesis (4-aminobenzonitriles), they might be expected to carry over to the case of rhodamines (K. A. Zachariasse, personal communication). The rhodamines and 4-aminobenzonitriles are similar in many respects. They both show no ICT reaction and no fluorescence quenching when the nitrogens are present as NH_2, NHAlk, or fixed amino rings. These authors present several arguments against the existence of a TICT state. The rate of formation of the ICT state does not decrease as the size of the bialkyl groups increases, as would be expected for a rotation of the bialkylamino group. It was found that the occurrence and efficiency of the ICT reaction with the 4-aminobenzonitriles depends on the nature of the amino substituent. The ICT efficiency decreases in the series $-N(C_2H_5)_2 > -N(CH_3)_2 > -NH(CH_3)$ (no ICT) and -NH2 (no ICT). In addition, with the nitrogen in rings of different sizes, the efficiency of ICT is in the order -piperidinyl (6) > pyrrodilinyl (5) > azetidinyl (4) > aziridinyl (3) (no ICT). This dependence can be correlated with the height of the inversion barrier of the amino groups, as deduced from dynamic NMR. For the fluorescence quenching of the rhodamines, a similar dependence of the reaction rate/efficiency on the nature of the amino substituent is observed. This then leads these authors to the assumption that the photophysical mechanism operating in the fluorescence quenching of the rhodamines is similar to that controlling the ICT reaction in the 4-aminobenzonitriles. Some of the compounds that have been considered to support the hypothesis of TICT states cannot be used as good tests of the authenticity of TICT states. For instance, there is no ICT and no dual fluorescence with fixed five- and six-membered rings, but there is an efficient ICT with a seven-membered ring, in which the amino group cannot rotate to become perpendicular to the ring. These authors also point out that if there were a TICT state, one would expect linear correlations between the charge transfer spectral maximum and the *IP*(D) and the peak oxidation potential of the donor; neither is found. This lack of correlation indicates that in the ICT state, the amino group (the donor) is strongly coupled to the benzonitrile group (the acceptor). This opposes the essential factor of the TICT hypothesis that the donor and acceptor groups are maximally decoupled in the final ICT state (the "principle of minimum overlap").

An alternative mechanism involving a solvent-induced two-level interaction with a promoting mode (amino N from pyramidal toward planar) was proposed (Zachariasse et al., 1993; von der Haar et al., 1995). This mechanism requires a sufficiently small energy gap between the two lowest excited singlet states, and a change in the configuration of the amino nitrogen from pyramidal toward planar as a promoting mode (see also next paragraph). The reader is referred to the original papers for a lucid discussion. If these arguments can also be applied to rhodamines, then the separate characteristics of the separate fluorescence components of TMRh-DNA might be due to modifications in the potential controlling the change in the configuration of the amino nitrogen from pyramidal toward planar, or to changes in the energy gap between the excited singlet states of the chromophore for the different TMRh-DNA complexes.

The ULM hypothesis

The influence of specific solvent interactions (especially alcohols) with the amine and carboxy moieties on the absorption and emission properties of rhodamines has been emphasized recently (see Arbeloa and Rohatgi-Mukherjee, 1986; Arbeloa et al., 1991a,b, and references therein). Based on solvent perturbation studies and on different derivatives of rhodamines, it has been suggested that an internal conversion leading to a mesomeric form with a higher fluorescence quantum yield can follow the excitation of rhodamine into the initial LE-ICT state; this mesomeric form has properties quite different from those of the proposed TICT state. In this model the positive charge in the xanthene-nitrogen $= N^+RR'$ is displaced into the ring system (to the nine-carbon atom of the ring) with a concomitant rotation of the amine group, leading to the pyramidal structure -N:RR'. This change from a planar to a pyramidal geometry is similar to the opening and closing of an umbrella, and therefore the new mesomeric state is called the ULM (umbrella-like movement) state. This ULM mesomeric structure can be stabilized by specific solvent interactions. The lone pair of the -N:RR' can act as a hydrogen bond acceptor (e.g., with alcohols) and the positive charge of $=N^+RR'$ can interact with an electron donor, such as the lone electron pairs of the hydroxyl groups of alcohols. The alkyl groups of methyl- and ethylamino rhodamines can also undergo hydrophobic interactions with the solvent. It has been proposed that this ULM mesomeric state contributes to a high quantum yield because the pyramidal structure does not necessarily lead to a rapid deactivation due to rotational motion of the amino groups or due to an insufficient orbital overlap with the Frank-Condon ground state. The charge of the COO^- group can stabilize the mesomeric structure of the dye where there is a partial positive charge at the nine-carbon atom of the xanthene ring. This interaction stabilizes the ULM mesomeric structure and is consistent with the increase in quantum yield for rhodamines with the carboxybenzyl group in the COO^- form, as opposed to the COOH and COOR forms. It is important to realize that the participation or stabilization of the ULM mesomeric struc-

ture leads to an increase in the fluorescence quantum yield, whereby for rhodamines the TICT state leads to a nonfluorescent state. These studies emphasize the critical effect that the charges, polarity, and hydrophobicity of the neighboring functional groups in the immediate environment of the rhodamines have on their fluorescence characteristics.

Steric hindrance of rotation about the amine-xanthene bond

It has been reported (Bergamasco et al., 1990) that RhB decays with two lifetimes in a mixture of glycerol and water ($\tau_{fast} \approx 0.85$ ns and $\tau_{slow} \approx$ 1.7–3.4 ns, depending on the wavelength of emission and the percentage of glycerol). For Rh101 there can be no rotation around the amine-xanthene bond, and these authors found that τ_{slow} is independent of the glycerol concentration. In addition, the lifetime of Rh101 does not depend on the temperature (Drexhage, 1973). These data are strong evidence that the extra-xanthene groups attached to the amine must be able to rotate around the amine-xanthene bond to increase the rate of internal conversion; if rotation around this bond is not available, this pathway of deactivation is blocked. This seems to be the case for the two fluorescent species of TMRh linked to DNA (see text).

Calculating steady-state fluorescence intensities for a mixture of two fluorescing components from lifetime data

For two fluorescent molecular species, A and B, the steady-state total fluorescence intensity (number of photons emitted per second) can be expressed as

$$F_{\text{steady state}} = N_A \cdot \phi_A + N_B \cdot \phi_B, \qquad \text{(A1)}$$

where N_A is the number of molecules A that are excited per unit time, ϕ_A is the quantum yield of A, and N_B and ϕ_B are the same quantities for species B.

By writing the quantum yields in terms of the rates of deactivation from the excited state, and expressing the fluorescence lifetimes in terms of these rates, it is easily shown that,

$$F_{\text{steady state}} = N_A \cdot \frac{\tau_f^A}{\tau_r^A} + N_B \cdot \frac{\tau_f^B}{\tau_r^B}. \qquad \text{(A2)}$$

τ_f^A and τ_r^A are the measured fluorescence lifetime and the radiative lifetime for species A; corresponding definitions hold for B. If the two species have the same radiative lifetimes, i.e., $\tau_r^A = \tau_r^B = \tau_r$, then we can write

$$F_{\text{steady state}} = N_{A+B} \cdot \left(\frac{1}{\tau_r}\right)\{a \cdot \tau_f^A + b \cdot \tau_f^B\}. \qquad \text{(A3)}$$

$N_{A+B} = N_A + N_B$ is the total number of molecules that are excited per unit time; $a = N_A/N_{A+B}$ and $b = N_B/N_{A+B}$ are the fractions of different species. The radiative rate is the rate of deactivation from the excited state in the absence of any other pathways of deactivation and is effectively independent of temperature, solvent conditions, etc., provided that the electronic structure of the molecule is not significantly perturbed.

Equilibrium equations corresponding to the reaction model in Fig. 1 for the salt and the temperature dependence of the TMRh-DNA complex

The binding of salt and the temperature dependence of the populations of double-stranded species can be analyzed by the reaction scheme in Fig. 1. The primed TMRh-DNA species refer to the low-salt forms of the helical dye-DNA complexes, and the corresponding unprimed species are those after binding to salt. The A and B species are fluorescent, and D is dark. The fluorescence lifetime for A is longer than that for B.

For species A′ and A, the bimolecular equilibrium with salt is

$$A' + n \cdot S \leftrightarrow A \qquad K_{A/S} = [A]/([A'] \cdot [S]^n) \approx [S_0]^{-n} \cdot ([A]/([A']). \qquad \text{(A4)}$$

Similar expressions apply for the B and D species. S is the interacting salt ion (Na^+).

For the monomolecular equilibria,

$$A \leftrightarrow B \; A' \leftrightarrow B', \text{ etc.}, \qquad \text{(A5)}$$

the equilibrium constants are defined by

$$K_{AB} = [B]/[A], \text{ etc., and } K_{A'B'} = [B']/[A'], \text{ etc.} \qquad \text{(A6)}$$

The subscripts identify the reaction for the equilibrium constants K. The monomolecular reactions A′ ↔ B′, etc., and A ↔ B shift to the right as the temperature increases. For all solutions used in this study, it is always true that $[S] \approx [S_0]$ ($[S_0]$ is the total concentration of salt). Only the A, B, A′, and B′ species are fluorescent; D and D′ are assumed to be "dark" states (nonfluorescent). As the salt concentration is raised, the species A′, B′, and D′ become depleted. The ratios [A]/[A′], [B]/[B′], and [D]/[D′], etc., are salt (Eqs. A5–A7) and temperature dependent (Figs. 5 and 6).

The total measured fluorescence, F_{tot}, can be written in terms of the fluorescence of all the emitting species. If we assume that $f_C = 0$, then

$$F_{tot} = [A]\{f_A + f_B \cdot K_{AB}\} + [A']\{f_{A'} + f_{B'} \cdot K_{A'B'}\} \qquad \text{(A7)}$$

or

$$F_{tot} = [A] \cdot \{\{f_A + f_B \cdot K_{AB}\} + ([S_0]^{-n}/K_{A/S}) \cdot \{f_{A'} + f_{B'} \cdot K_{A'B'}\}\}. \qquad \text{(A8)}$$

The small fs are the fluorescence intensities per molar concentration of this species. Most experiments are done with sufficient salt so that $F_{tot} \approx [A] \cdot \{f_A + f_B \cdot K_{AB}\}$. The fs can also be temperature dependent. As the temperature increases, the dark state (D) becomes more populated and the fluorescent species decrease. It is to a large extent due to the transition from the fluorescence states to the dark state that the fluorescence intensity decreases dramatically as the temperature isincreased;inaddition,$\phi_B < \phi_A$.

For TMRh-DNA the salt titrations behave as predicted by a one-step bimolecular reaction with an overall equilibrium constant of K_{obs}; however, because K_{obs} is a combination of fundamental reaction equilibrium constants, the van't Hoff plot cannot be analyzed in terms of fundamental reaction steps. We have determined the equilibrium constant K_{AB} between 5°C and 60°C from the fluorescence lifetime results (see above).

We thank D. M. J. Lilley, A. I. H. Murchie, and F. Stühmeier for many discussions and collaborations on related topics; A. Zechel and T. Stafforst for excellent technical assistance; E. Jares-Erijman, L. Erijman, G. Vereb, J. Szöllôsi, and T. M. Jovin for helpful criticism of the manuscript; K. A. Zachariasse for helpful discussions concerning intramolecular charge transfer; and S. Damjanovich for suggesting the collaboration between the authors.

REFERENCES

Arbeloa, F. L., I. U. Aguirresacona, and I. L. Arbeloa. 1989. Influence of the molecular structure and the nature of the solvent on the absorption and fluorescence characteristics of rhodamines. *Chem. Phys.* 130: 371–378.

Arbeloa, F. L., T. L. Arbeloa, M. J. T. Estévez, and I. L. Arbeloa. 1991a. Photophysics of rhodamines. Molecular structure and solvent effects. *J. Phys. Chem.* 95:2203–2208.

Arbeloa, T. L., M. J. T. Estévez, F. L. Arbeloa, I. U. Aguirresacona, and I. L. Arbeloa. 1991b. Luminescence properties of rhodamines in water/ethanol mixtures. *J. Lumin.* 48–49:400–404.

Arbeloa, F. L., and K. K. Rohatgi-Mukherjee. 1986. Solvent effects on the photophysics of the molecular forms of rhodamine B. Internal conversion mechanism. *Chem. Phys. Lett.* 129:607–614.

Arndt-Jovin, D. J., and T. M. Jovin. 1990. Multivariate chromosome analysis and complete karyotyping using dual labeling and fluorescence digital imaging microscopy. *Cytometry.* 11:80–93.

Bauman, J., G. Calzaferri, L. Forss, and T. Hugentobler. 1985. Wavelength-dependent fluorescence decay: an investigation by multiple-frequency picosecond phase fluorometry. *J. Photochem.* 28:457–473.

Beaucage, S. L., and M. H. Caruthers. 1981. Deoxynucleoside phosphoramidites—a new class of key intermediates for deoxypolynucleotide synthesis. *Tetrahedron Lett.* 22:1859–1862.

Bergamasco, S., G. Calzaferri, and K. Hädener. 1990. Solute-solvent relaxation of electronically excited xanthene dyes. *J. Photochem. Photobiol. A. Chem.* 53:109–125.

Birks, J. B. 1975. Organic Molecular Photophysics. John Wiley and Sons, New York. 409–613.

Boltz, R. C., P. A. Fischer, L. S. Wicker, and L. B. Peterson. 1994. Single UV excitation of Hoechst 33342 and ethidium bromide for simultaneous cell cycle analysis and viability determinations on in vitro cultures of murine B lymphocytes. *Cytometry.* 15:28–34.

Breslauer, K. J., R. Frank, H. Blocker, and L. A. Marky. 1986. Predicting DNA duplex stability from the base sequence. *Proc. Natl. Acad. Sci. USA.* 83:3746–3750.

Bresloff, J. L., and D. M. Crothers. 1975. DNA-ethidium reaction kinetics: demonstration of direct ligand transfer between DNA binding sites. *J. Mol. Biol.* 95:103–123.

Cardullo, R. A., S. Agrawal, C. Flores, P. C. Zamecnik, and D. E. Wolf. 1988. Detection of nucleic acid hybridization by nonradiative fluorescence resonance energy transfer. *Proc. Natl. Acad. Sci. USA.* 85: 8790–8794.

Chang, T.-L., and W. L. Borst. 1990. Effect of solvent polarity on a rotational isomerization mechanism of rhodamine-B in normal alcohols. *J. Chem. Phys.* 93:4724–4729.

Clegg, R. M. 1992. Fluorescence resonance energy transfer and nucleic acids. *Methods Enzymol.* 211:353–388.

Clegg, R. M. 1995. Fluorescence resonance energy transfer. *Curr. Opin. Biotechnol.* 6:102–110.

Clegg, R. M. 1996. Fluorescence resonance energy transfer. *In* Fluorescence Imaging Spectroscopy and Microscopy. X. F. Wang and B. Herman, editors. John Wiley and Sons, New York. 179–252.

Clegg, R. M., A. I. H. Murchie, and D. M. J. Lilley. 1993. The four-way DNA junction: a fluorescence resonance energy transfer study. *Braz. J. Med. Biol. Res.* 26:405–416.

Clegg, R. M., A. I. H. Murchie, and D. M. J. Lilley. 1994. The solution structure of the four-way DNA junction at low-salt conditions: a fluorescence resonance energy transfer analysis. *Biophys. J.* 66:99–109.

Clegg, R. M., A. I. H. Murchie, A. Zechel, C. Carlberg, S. Diekmann, and D. M. J. Lilley. 1992. Fluorescence resonance energy transfer analysis of the structure of the four-way junction. *Biochemistry.* 31:4846–4856.

Clegg, R. M., A. I. H. Murchie, A. Zechel, and D. M. J. Lilley. 1993. Observing the helical geometry of double-stranded DNA in solution by fluorescence resonance energy transfer. *Proc. Natl. Acad. Sci. USA.* 90:2994–2998.

Connolly, B. A. 1987. The synthesis of oligonucleotides containing a primary amino group at the 5′ terminus. *Nucleic Acids Res.* 15: 3131–3139.

Cooper, J. P., and P. J. Hagerman. 1990. Analysis of fluorescence energy transfer in duplex and branched DNA molecules. *Biochemistry.* 29: 9261–9268.

Corrie, J. E., and J. S. Craik. 1994. Synthesis and characterization of pure isomers of iodoacetamidotetramethylrhodamine. *J. Chem. Soc. (Perkin Trans. 1).* 1:2967–2973.

Demas, J. N., and G. A. Crosby. 1971. The measurement of photoluminescence quantum yields. A review. *J. Phys. Chem.* 75:991–1024.

Dougherty, G., and W. J. Pigram. 1982. Spectroscopic analysis of drug-nucleic acid interactions. *CRC Crit. Rev. Biochem.* 12:103–132.

Drexhage, K. H. 1973. Structure and properties of laser dyes. *In* Dye Lasers. F. P. Schäfer, editor. Springer, Berlin. 144–193.

Eis, P. S., and D. P. Millar. 1993. Conformational distributions of a four-way DNA junction revealed by time-resolved fluorescence resonance energy transfer. *Biochemistry.* 32:13852–13860.

Ferguson, J., and A. W.-H. Mau. 1973. Spontaneous and stimulated emission from dyes. Spectroscopy of the neutral molecules of acridine orange, proflavin, and rhodamine B. *Aust. J. Chem.* 26:1617–24.

Förster, T. 1951. Fluoreszenz Organischer Verbindungen. Vandenhoeck and Ruprecht, Göttingen. 312.

Förster, T., and G. Hoffmann. 1971. Die Viskositätsabhängigkeit der Fluoreszenzquantenausbeuten einiger Farbstoffsysteme. *Z. Phys. Chemie Neue Folge.* 75:63–76.

Gohlke, C., A. I. H. Murchie, D. M. J. Lilley, and R. M. Clegg. 1994. Kinking of DNA and RNA helices by bulged nucleotides observed by fluorescence resonance energy transfer. *Proc. Natl. Acad. Sci. USA.* 91:11660–11664.

Grabowski, Z. R., K. Rotkiewicz, A. Siemiarczuk, D. J. Cowley, and W. Baumann. 1979. Twisted intramolecular charge transfer states (TICT). A new class of excited states with a full charge separation. *Nouv. J. Chim.* 3:443–454.

Gratton, E., D. M. Jameson, N. Rosato, and G. Weber. 1984. Multifrequency cross-correlation phase fluorometer using synchroton radiation. *Rev. Sci. Instrum.* 55:486–494.

Haas, E., and E. Katchalski-Katzir. 1978. Effect of the orientation of donor and acceptor on the probability of energy transfer involving electronic transitions of mixed polarization. *Biochemistry.* 17:5064–5070.

Haugland, R. P. 1992. Molecular Probes Inc.: Handbook of Fluorescent Probes and Research Chemicals, 5th ed., Eugene. 1–421.

Hirons, G. T., J. J. Fawcett, and H. A. Crissman. 1994. TOTO and YOYO: new very bright fluorochromes for DNA content analyses by flow cytometry. *Cytometry.* 15:129–140.

Hochstrasser, R. A., S. M. Chen, and D. P. Millar. 1992. Distance distribution in a dye-linked oligonucleotide determined by time-resolved fluorescence energy transfer. *Biophys. J.* 45:133–141.

Jakobi, H., and H. Kuhn. 1962. Richtigungen der Übergangsmomente der Absorptionsbanden von Acridin-, Phenazin-, Phenoxazin- und Xanthenfarbstoffen aus Dichroismus und Fluoreszenzpolarization. *Z. Elektrochem.* 66:46–53.

Jameson, D. M., E. Gratton, and R. D. Hall. 1984. The measurement and analysis of heterogenous emissions by multifrequency phase and modulation fluorometry. *Appl. Spectrosc. Rev.* 20:55–106.

Jares-Erijman, E. A., and T. M. Jovin. 1996. Determination of DNA helical handedness by fluorescence resonance energy transfer. *J. Mol. Biol.* 257:597–617.

Karstens, T., and K. Kobs. 1980. Rhodamine B and rhodamine 101 as reference substances for fluorescence quantum yield measurements. *J. Phys. Chem.* 84:1871–1872.

Kemnitz, K., N. Tamai, I. Yamazaki, N. Nakashima, and K. Yoshihara. 1986. Fluorescence decays and spectral properties of rhodamine B in submono-, mono-, and multilayer systems. *J. Phys. Chem.* 90: 5094–5101.

Kuhn, H. 1959. Neuere Untersuchungen über das Elektronengasmodell organischer Farbstoffe. *Angew. Chem.* 71:93–101.

Lakowicz, J. R. 1983. Principles of Fluorescence Spectroscopy. Plenum Press, New York. 496.

LePecq, J.-B., and C. Palotti. 1967. A fluorescent complex between ethidium bromide and nucleic acids: physical-chemical characterization. *J. Mol. Biol.* 27:87–106.

Lilley, D. M. J., and R. M. Clegg. 1993. The structure of branched DNA species. *Q. Rev. Biophys.* 26:131–175.

Löber, G. 1981. The fluorescence of dye-nucleic acid complexes. *J. Lumin.* 22:221–265.

Loontiens, F. G., L. W. McLaughlin, S. Diekmann, and R. M. Clegg. 1991. Binding of Hoechst 33258 and 4′,6-diamidino-2-phenylindole to self-

complementary decadeoxynucleotides with modified exocyclic base substituents. *Biochemistry.* 30:182–189.

Loontiens, F. G., P. Regenfuss, A. Zechel, L. Dumortier, and R. M. Clegg. 1990. Binding characteristics of Hoechst 33258 with calf thymus DNA, poly[d(AT)], and d(CCGGAATTCCGG): multiple stoichiometries and determination of tight binding with a spectrum of site affinities. *Biochemistry.* 29:9029–9039.

Macgregor, R. B., R. M. Clegg, and T. M. Jovin. 1985. Pressure-jump study of the kinetics of ethidium bromide binding to DNA. *Biochemistry.* 24:5503–5510.

Macgregor, R. B., R. M. Clegg, and T. M. Jovin. 1987. Viscosity dependence of ethidium-DNA intercalation kinetics. *Biochemistry.* 26: 4008–4016.

Manning, G. S. 1979. Counterion binding in polyelectrolyte theory. *Acc. Chem. Res.* 12:443–449.

Mergny, J.-L., A. S. Boutorine, T. Garestier, G. Belloc, M. Rougée, N. V. Bulychev, A. A. Koshkin, J. Bourson, A. V. Lebedev, B. Valeur, N. T. Thuong, and C. Hélène. 1994. Fluorescence energy transfer as a probe for nucleic acid structures and sequences. *Nucleic Acids Res.* 22: 920–928.

Morrison, L. E., T. C. Halder, and L. M. Stols. 1989. Solution-phase detection of polynucleotides using interacting fluorescent labels and competitive hybridization. *Anal. Biochem.* 183:231–244.

Murchie, A. I. H., R. M. Clegg, E. von Kitzing, D. R. Duckett, S. Dieckmann, and D. M. J. Lilley. 1989. Fluorescence energy transfer shows that the four-way DNA junction is a right-handed cross of antiparallel molecules. *Nature.* 341:763–766.

Parkhurst, K. M., and L. J. Parkhurst. 1993. Kinetic studies of oligonucleotide-DNA hybridization in solution by fluorescence resonance energy transfer. *Biophys. J.* 64:A266. (Abstr.)

Penzkofer, A., and M. Falkenstein. 1978. Theoretical investigation of amplified spontaneous emission with picosecond light pulses in dye solutions. *Opt. Quant. Electron.* 10:399–423.

Piston, D. W., G. Marriott, T. Radivoyevich, R. M. Clegg, T. M. Jovin, and E. Gratton. 1989. Wide-band acousto-optic light modulator for frequency domain fluorometry and phosphorimetry. *Rev. Sci. Instrum.* 60:2596–2600.

Record, T. M., Jr., C. F. Anderson, and T. M. Lohman. 1978. Thermodynamic analysis of ion effects on the binding and conformational equilibria of proteins and nucleic acids: the roles of ion association or release, screening, and ion effects on water activity. *Q. Rev. Biophys.* 11:103–178.

Rettig, W. 1986. Ladungstrennung in angeregten Zuständen entkoppelter Systeme—TICT-Verbindungen und Implikationen für die Entwicklung neuer Laserfarbstoffe sowie für den Primärprozess von Sehvorgang und Photosynthese. *Angew. Chem.* 98:969–986.

Römpp, H., and H. Raaf. 1982. Organische Chemie im Probierglass. Kosmos, Stuttgart. 252.

Ryan, D. P., and D. M. Crothers. 1984. Relaxation kinetics of DNA-ligand binding including direct transfer. *Biopolymers.* 23:537–562.

Sauer, M., R. Han, R. Müller, A. Schulz, R. Taddy, S. Seeger, J. Wolfrum, J. Arden-Jacob, G. Deltau, N. J. Marx, and K. H. Drexhage. 1993. New fluorescent labels for time-resolved detection of biomolecules. *J. Fluoresc.* 3:131–139.

Schurr, J. M., B. S. Fujimoto, P. Wu, and S. Song. 1992. Fluorescence studies of nucleic acids: dynamics, rigidities, and structures. *In* Topics in Fluorescence Spectroscopy: Biochemical Applications. J. R. Lakowicz, editor. Plenum Press, New York. 137–227.

Selvin, P. R. 1995. Fluorescence resonance energy transfer. *Methods Enzymol.* 246:300–334.

Selvin, P. R., and J. E. Hearst. 1994. Luminescence energy transfer using a terbium chelate: improvements on fluorescence energy transfer. *Proc. Natl. Acad. Sci. USA.* 91:10024–10028.

Selvin, P. R., T. M. Rana, and J. E. Hearst. 1994. Luminescence resonance energy transfer. *J. Am. Chem. Soc.* 116:6029–6030.

Sixou, S., F. C. Szoka, Jr., G. A. Green, B. Giusti, G. Zon, and D. J. Chin. 1994. Intracellular oligonucleotide hybridization detected by fluorescence resonance energy transfer (FRET). *Nucleic Acids Res.* 22: 662–668.

Snare, M. J., F. E. Treloar, K. P. Ghiggino, and P. J. Thistlethwaite. 1982. The photophysics of rhodamine B. *J. Photochem.* 18:335–346.

Soumpasis, D. M., A. Garcia, R. Klement, and T. M. Jovin. 1990. The potentials of mean force (PMF) approach for treating ionic effects on bimolecular structures in solution. *In* Theoretical Biochemistry and Molecular Biophysics. D. L. Beveridge and R. Lavery, editors. Adenine Press, New York. 343–360.

Steiner, R. F., and Y. Kubota. 1983. Fluorescent dye-nucleic acid complexes. *In* Excited States of Biopolymers. R. F. Steiner, editor. Plenum Press, New York. 203–254.

Stoll, V. S., and J. S. Blanchard. 1990. Buffers: principles and practice. *Methods Enzymol.* 182:24–38.

Tuschl, T., C. Gohlke, T. M. Jovin, E. Westhof, and F. Eckstein. 1994. A three-dimensional model for the hammerhead ribozyme based on fluorescence measurements. *Science.* 266:785–789.

von der Haar, T., A. Hebecker, Y. Il'ichev, Y. B. Jiang, W. Kühnle, and K. A. Zachariasse. 1995. Excited-state intramolecular charge transfer in donor/acceptor-substituted aromatic hydrocarbons and in biaryls. The significance of the redox potentials of the D/A subsystems. *Recl. Trav. Chim. Pays-Bas.* 114:430–442.

Vogel, M., W. Rettig, R. Sens, and K. H. Drexhage. 1988. Structural relaxation of rhodamine dyes with different N-substitution patterns: a study of fluorescence decay times and quantum yields. *Chem. Phys. Lett.* 147:452–460.

Voss, E. W. 1984. Fluorescein Hapten: An Immunological Probe. CRC Press, Boca Raton. 193.

Wu, P., and L. Brand. 1992. Orientation factor in steady-state and time-resolved resonance energy transfer measurements. *Biochemistry.* 31: 7939–7947.

Zachariasse, K. A., T. von der Haar, A. Hebecker, U. Leinhos, and W. Kühnle. 1993. Intramolecular charge transfer in amino-benzonitriles: requirements for dual fluorescence. *Pure Appl. Chem.* 65:1745–1750.

Zimmer, C., and U. Wähnert. 1986. Nonintercalating DNA-binding ligands: specificity of the interaction and their uses as tools in biophysical, biochemical and biological investigations of the genetic material. *Prog. Biophys. Mol. Biol.* 47:31–112.